Wave breaking in long wave models and undular bores

Master thesis in Applied and Computational Mathematics

Mats K. Brun

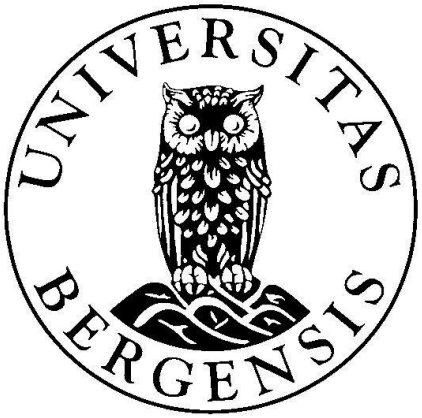

Department of Mathematics
University of Bergen
December 18, 2015

Preface

This is my masters thesis in applied mathematics, and also my final work as a student at the University of Bergen, Norway. I would like to thank my advisor, Professor Henrik Kalisch, for invaluable input and guidance along the way, and also Professor Magnus Svärd for helping to implement the SBP-SAT numerical method, in addition to some of the related theory.

All computations and figures in this report were done using MatLab v. R-2013b.

Contents

List of Figures

Chapter 1

Indroduction

Bores are a well known phenomena in fluid mechanics, although their occurrence in nature is relatively rare. The circumstances in which they occur is usually when a tidal swell causes a difference in surface elevation in the mouth of a river, or narrow bay, causing long waves to propagate upstream. The term 'tidal bore' is also frequently used in this context. Depending on the conditions the bore may take on various forms, ranging from a smooth wavefront followed by a smaller wave train, to one singe breaking wavefront. Some noteworthy locations where tidal bores can be found include the River Seine in France, the Petitcodiac River in Canada, and the Qiantang River in China. Common for all these locations is a large tidal range. Bores, when powerful enough, can produce particularly unsafe environments for shipping, but at the same time popular opportunities for river surfing.

As found by Favre in 1935 [7] by wave tank experiments, the strength of the bore can be determined by the ratio of the incident water level above the undisturbed water depth to the undisturbed water depth. Denoting this ratio by α, bores can occur in one of three categories: If α is less than 0.28 the bore is purely undular, and will feature oscillations downstream of the bore front. If α is between 0.28 and 0.75 the bore will continue to feature oscillations, but one or more waves behind the bore front will start to break. If α is greater than 0.75 the bore is completely turbulent, and can no longer be described by the standard potential flow theory.

The goal of this report is to simulate the time evolution of an undular bore through numerical experiments, using a dispersive nonlinear shallow water theory, in particular the Korteweg-deVries (KdV) equation. This is a third order nonlinear partial differential equation, where the dependent variable describes the displacement of the free surface. When deriving this equation,

an expression for the velocity field of the flow is also available. This can be calculated at any point in the fluid, as long as the displacement of the surface is known. Thus, solving the KdV equation also yields the fluid particle velocity field, which can be used to calculate fluid particle trajectories, as done by Bjørkvåg and Kalisch [17], but also to formulate a breaking criterion [3]. By applying this breaking criterion to the undular bore, the onset of breaking, and thus also a maximum allowable wave height (due to the nonlinearity of the model equation), can be computed numerically. This criterion can also be applied to the exact traveling wave solutions of the KdV equation, namely the 'solitary wave' solution and the 'cnoidal wave' solution. These are waves of constant shape traveling at constant velocity, thus applying the breaking criterion yields a maximum height for which they can exist.

The theory leading to the formulation of the KdV equation is also included, in addition to formulation of the linearized and shallow water equations. These, however, serve only as 'stepping stones' towards the higher order Boussinesq equations, and are not used in any further calculations.

1.1 Some historical notes

The first successful description of surface gravity waves on water using a flow potential was done by George Biddell Airy in 1841 [9]. This is a linear theory, in which wave propagation only transfers energy in the propagation direction. Airy's linear theory was later extended by George Stokes in 1847 [8], to include nonlinear wave motion. In Stokes' nonlinear theory, the propagating waves transfers both energy and mass in the propagation direction, in addition to having an amplitude dependent frequency dispersion. This amplitude dependency is the key to important qualitative changes in the behavior of waves compared to those described by the linear theory, and thus a wider range of observed phenomena could be explained with Stokes' theory.

However, Stokes' nonlinear theory fails to describe correctly the behavior of long waves, or waves on a shallow body of water. In particular, it predicts that long waves of appreciable amplitude (as compared to water depth) can not propagate without altering shape. John Scott Russell's description of the solitary wave in 1844 [16], was therefore hard to accept for Airy and Stokes, as this could travel large distances while maintaining a constant shape. This problem remained unsolved for decades, until an explanation was provided by Joseph Boussinesq in 1871 [10], and then again independently by Lord Rayleigh in 1876 [12]. They found that the nonlinear effects, causing long

waves to change shape, may be balanced by effects of dispersion. Today, it is recognized that Stokes' equations are applicable on deep to intermediate depths, while the Boussinesq equations are needed for shallow water.

Diederik Korteweg and Gustav deVries were then the first to find the solitary wave as a solution of an equation in 1895 [13], the equation now known as the KdV equation. They also managed to derive the more general periodic 'cnoidal' solution. After this, investigation of the KdV equation mostly died out until the invention of computers and advancements in numerical methods. Not until 1965 did Zabusky and Kruskal discover through numerical experiments that solutions of the KdV equation decomposed at large times into a train of solitary waves [14]. They also found that the shape of these waves were almost unaffected by passing through each other. A few years later, in 1967, the full analytical solution of the KdV equation was found by Gardner, Greene, Kruskal and Miura [15], using a method they called 'the inverse scattering transform'.

The first descriptions of the solitary wave, and subsequently explicit mathematical formulation of these, has lead to the modern physical theory of 'solitons' (a more general notion of a solitary wave), which today has a wide range of applications in physics aside from fluid mechanics. The KdV equation is also a widely recognized model equation for long, unidirectional waves, and is still a subject of great interest both in the fields of mathematics and in physics. For instance, the fact that it can be solved exactly makes it a good way to test the accuracy of numerical methods.

1.2 Outline of the report

We begin this report by establishing some basic properties of surface gravity waves, and then go on to describe the physical system in which the wave motion takes place. The assumptions made on the fluid flow are also given, in addition to some brief justification of these. The governing equations and boundary conditions of the flow are then given, and the full surface gravity wave problem in two spatial dimensions is stated.

This system of equations is then linearized and solved exactly, yielding the linear surface gravity wave equations, valid for waves of small amplitude. Further, we assume a shallow body of water and see how this affects the linear equations. This information is then used to derive the nonlinear shallow water equations and the Boussinesq system of equations, as limiting cases of

the full surface gravity wave problem.

When deriving the Boussinesq equations, a particular scaling regime is also imposed, yielding a certain range of relative wavelengths for which the approximation is valid. Continuing with this Boussinesq scaling regime, the KdV equation is derived and traveling wave solutions of this are found analytically. The horizontal component of the velocity field of the fluid flow is then used to formulate a breaking criterion for surface gravity waves in the Boussinesq parameter regime, and this is applied to the exact traveling wave solutions.

Next, two different numerical schemes for solving the KdV equation is explained, in addition to some analysis of their respective stability properties. Numerical experiments are then used together with the breaking criterion to determine the onset of breaking in the bore, in which the ratio $\alpha > 0.28$ is under review. We then calculate the maximum wave heights of the bore and corresponding breaking times for several values of α. This is then compared to the results obtained for the exact solutions.

Finally, a summary of the results and some discussion around these are presented. The source code for the numerical schemes may be found in the appendix.

1.3 Notation

The notation used in this report is fairly standard, but nevertheless, some comments on this are provided here:

A bold font will always indicate a vector, for instance $\mathbf{u} = (u, v)$, which denotes the velocity field.

The differential operator $\frac{D}{Dt} = \frac{\partial}{\partial t} + \mathbf{u} \cdot \nabla$ denotes the material or total derivative.

Unless otherwise stated, subscripts will denote partial derivatives, for instance: $\eta_x = \frac{\partial \eta}{\partial x}$. These two notations will be used interchangeably.

Chapter 2

The physical system and assumptions

2.1 Basic wave theory

In this section some basic theory on waves will be presented, along with establishing some parameters that will be important later on. Although there are several types of waves commonly considered in the field of fluid mechanics, e.g. compression waves, internal waves, etc., the discussion in this report is limited to the study of interface waves.

We start by defining the following:
- wavelength: λ, the distance over which the wave's shape repeats
- horizontal wavenumber: k, the number of cycles per unit distance in the horizontal direction
- circular frequency: ω, the angular displacement per unit time
- period: T, the amount of time for the wave to travel one wavelength
- phase shift: x_0, denotes the position of the crest/trough at time $t = 0$
- phase speed: c_p, the velocity with which one point on the wave profile is moving
- group speed: c_g, the velocity with which the overall shape (envelope) of the wave profile is moving

In addition, we also have the following relations between these parameters:

$$\lambda = \frac{2\pi}{k},\ \omega = \frac{2\pi}{T},\ c_p = \frac{\omega}{k},\ c_g = \frac{\partial \omega}{\partial k} \tag{2.1}$$

The simplest description of a smooth repetative oscillation of a one dimensional surface, where the amplitude, a_0, is not too large, is given by a single sinusoid:

$$\eta(x,t) = a_0 \cos(kx - \omega t - x_0) \tag{2.2}$$

When the governing equations and boundary conditions are linear, the principle of superposition can be used on the sinusoidal waves. In this way they can be used to construct any periodic waveform, as stated in Fourier's theorem. However, in the linear theory, trajectories of the fluid particles form closed curves, and there is no mean velocity of the fluid particles. In the nonlinear theory there is still an orbital motion of the fluid particles, but the curves need not be closed (i.e. Stokes drift). Thus, the linear theory is insufficient for the purpose of formulating a breaking criterion.

For one single sinusoidal wave, the angular frequency is proportional to the wavenumber, and the propagation speed is given by $c = \frac{\lambda}{T}$. Interference of several sinusoidal waves with slightly different wavelengths, but the same amplitude and propagation direction will however result in a wave group where waves of different wavelength travel at different phase speeds. Thus arises the need for the distinction between phase speed and group speed, since the velocity of the composed wave is not uniquely defined, as opposed to the single sinusoid case. The waves are in this case said to be 'dispersive', and the relationship between ω and k is called the 'dispersion relation'. Dispersion is a property of the medium in which the waves are traveling rather than the waves themselves. A famous example is refraction of white light through a dispersive prism, where the different colors refract at different angles, splitting white light into a rainbow.

When ω is a linear function of k, without being directly proportional, the wave envelope will travel at a single velocity and retain its shape as the wave packet propagates. The individual peaks within the envelope will travel at the phase speed. If there is a nonlinear relationship between ω and k the envelope will not move at a single velocity, and its shape will become distorted as it travels.

2.2 The physical system

The goal of this section is to establish a simplified description of a physical system in which waves propagate along one coordinate axis. Such as a wave

tank in a laboratory where there is no bottom topography to affect the flow. We use a non-rotating cartesian coordinate system with the x-axis along the horizontal direction, and the y-axis along the vertical direction. The unit vectors in the x and y directions will be denoted by $\mathbf{i}$ and $\mathbf{j}$, respectively, and time by $t \geq 0$.

Consider a narrow and shallow canal filled with a body of fluid (water), separated by a massless interface with the air above it. The canal stretches out in each direction along the x-axis, and has a horizontal flat bottom of constant depth h_0. Assume the canal is narrow enough that we can neglect all transverse motion of the fluid, hence the use of only two spatial coordinates. The equilibrium level of the free surface is set to $y = 0$ and the bottom at $y = -h_0$.

The free surface and pressure of the fluid are described respectively by the single valued functions:

$$y = \eta(x, t) \quad \text{and} \quad p(x, y, t) \tag{2.3}$$

And the velocity field of the flow by the vector valued function:

$$\mathbf{u}(x, y, t) = (u, v)^T \tag{2.4}$$

where u is the horizontal velocity component, and v is the vertical velocity component.

This system is illustrated in the figure below:

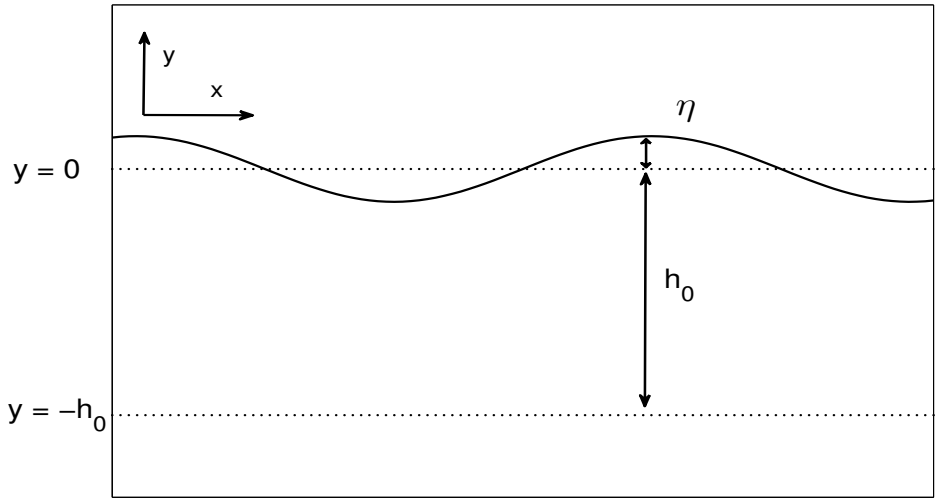

Figure 2.1: Reference system

We assume gravity is the only external force acting on the body of water, and that the gravitational field is constant. Since the density of water is much greater than that of air, we also assume there is no change in air pressure such that the pressure above the body of water is constant. Thus, we denote by the constants g and p_0 the gravitational acceleration and the undisturbed pressure in the air, respectively. The length scales of the wave motion considered are relatively long, such that any effects of surface tension can be ignored, but also short enough that any large scale phenomena such as the Coriolis force can be neglected. A few scaling arguments are provided:

Surface tension in a fluid will act as a restoring force on the free surface, and although water has a high surface tension (due to cohesion) when compared to most other fluids, this is only apparent for very small length scales. For waves affected by surface tension the dispersion relation is given by:

$$\omega = (g + \frac{\sigma}{\rho}k^2)k \tanh(kh_0) \tag{2.5}$$

where the σ denotes the surface tension of the fluid, and ρ the density.

Since wavenumber and wavelength are inversely proportional, increasing the wavelength will cause the surface tension term to decrease rapidly in size. The term "capillary-gravity waves", or "ripples", are used when the

wavelength is small enough such that this term is significant. The typical wavelength of these waves is less than a few centimeters in case of a water-air interface. For even shorter wavelengths, around a few millimeters, surface tension becomes the dominating restoring force and the effects of gravity are negligible.

On the other hand, for physical systems with very large length scales (e.g. tidal motion), the Earth's rotation has to be taken into account to model it correctly. Whether or not this is the case depends on the size of the Rossby number, given by:

$$R_0 = \frac{U}{fl} \tag{2.6}$$

where U is the magnitude of the mean velocity, l is the typical length scale, and f is the Coriolis parameter (constant for a given latitude).

A small Rossby number signifies a system which is strongly affected by the Coriolis force, and since the parameter f is typically of the order 10^{-5}, the length scales need to be correspondingly large for this to be the case.

2.3 Assumptions on the flow

We assume the body of fluid is initially at rest, and that the fluid flow is ideal, that is incompressible, irrotational, and inviscid. Although no real fluid can satisfy these criteria, the theory of an ideal flow can still accurately predict a real flow under certain circumstances. Note also that assuming the flow to be ideal is not the same as assuming the fluid itself to be ideal, although it shall be seen in the next chapter that for the sake of derivation it makes no difference.

A fluid flow may be considered inviscid when momentum forces are much greater than viscous forces. This is usually stated in terms of the Reynolds number, which is defined by:

$$Re = \frac{Ul}{\nu} \tag{2.7}$$

where ν is the kinematic viscosity of the fluid.

A Reynolds number much greater than one is equivalent of saying that viscous effects are negligible. For water ν is of the order 10^{-5} so unless very small length scales are considered this will most likely be the case. However, in the presence of a boundary layer near solid boundaries, viscosity plays a

more dominant role than in the bulk part of the flow, but for a low viscosity fluid (such as water) this only concerns a very narrow region and has little influence on the shape of the surface.

For an incompressible flow we have that the density of a given fluid parcel does not change as it moves in the flow field through regions of varying pressure. The mathematical way of stating this is:

$$\frac{D\rho}{Dt} = 0 \tag{2.8}$$

Thus the density ρ may vary from one point in space to another. However, since the fluid is initially at rest and the depth is not too large, we also assume that the initial density distribution of the fluid is uniform throughout space. Hence, in the following ρ will be treated as a constant.

Irrotational flow is a flow in which there is no net rotation on a given fluid element from one instant in time to another as it moves in the flow field. For a body of fluid initially at rest, rotation of a fluid particle can only be caused by a torque applied by shear forces, and in an incompressible and inviscid flow all such forces are abscent. Thus, the flow will remain irrotational forever as long as the initial state is rotation free. This is also stated in Kelvin's circulation theorem. Generally when a flow is viscid or compressible, it also becomes rotational.

After the governing equations are established during the next section, it shall be seen that some of these arguments are redundant.

Chapter 3

Theory

3.1 Governing equations

In this section we give the governing equations for the fluid flow under the assumptions previously established. These can also be found in chapter 13 of [1], for instance.

By applying Newton's second law of motion to an infinitesimal fluid parcel moving in the flow field we get an equation for the conservation of momentum, known as Euler's equation in two spatial variables:

$$\frac{D\mathbf{u}}{Dt} = \frac{\partial \mathbf{u}}{\partial t} + (\mathbf{u} \cdot \nabla)\mathbf{u} = -\frac{1}{\rho}\nabla p - g\mathbf{j} \tag{3.1}$$

This equation can be seen as a special case of the Navier-Stokes' equation when the viscous term is negligible.

We also have that the net flux of fluid in a given control volume must be equal to zero, and this gives the equation for conservation of mass, known as the continuity equation:

$$\frac{\partial \rho}{\partial t} + \nabla \cdot (\rho \mathbf{u}) = 0 \tag{3.2}$$

which in this case simplifies to:

$$\nabla \cdot \mathbf{u} = 0 \tag{3.3}$$

due to (2.8). Hence, the flow is divergence-free, which is just another way of stating that the initial density distribution will remain constant in time. This is because it can be seen that the divergence of the fluid velocity, at a given point in space, specifies the rate of change in the volume of an infinitesimal

fluid element, at that point, which is following the flow, i.e. $\frac{1}{\delta V}\frac{DV}{Dt} = \nabla \cdot \mathbf{u}$.

We continue by defining the vorticity of the flow, a vector that describes the local rotary motion at a point in the fluid:

$$\omega = \nabla \times \mathbf{u} \tag{3.4}$$

and since we previously assumed the flow to be irrotational we can write:

$$\omega = 0 \tag{3.5}$$

By rewriting the Euler equation (3.1) in terms of ω we get:

$$\frac{\partial \mathbf{u}}{\partial t} + \nabla(\frac{1}{2}\mathbf{u}^2) + \omega \times \mathbf{u} = -\frac{1}{\rho}\nabla p - g\mathbf{j} \tag{3.6}$$

and by taking the curl of this equation we eliminate the pressure gradient and get the vorticity equation:

$$\frac{\partial \omega}{\partial t} + \nabla \times (\omega \times \mathbf{u}) = 0$$

by applying equation (3.3) it can also be written as:

$$\frac{\partial \omega}{\partial t} + (\mathbf{u} \cdot \nabla)\omega = (\omega \cdot \nabla)\mathbf{u} \tag{3.7}$$

From here it is easy to see that $\omega = 0$ is a possible solution, thus, if $\omega = 0$ initially it will remain so for all time (also assuming $\nabla \mathbf{u}$ is bounded).

In other words, the Euler equation may allow for rotation but only if the initial state of the flow includes rotation.

In the Navier-Stokes' equation the viscous term is given by $\mu\nabla^2\mathbf{u}$, where $\mu = \rho\nu$ is the dynamic viscosity of the fluid. By rewriting the second factor as: $\nabla^2\mathbf{u} = \nabla(\nabla \cdot \mathbf{u}) - \nabla \times (\nabla \times \mathbf{u})$, we immediatly see from (3.3) and (3.5) that this term drops out. Thus an irrotational and incompressible flow is automatically inviscid, just as expected.

Further, equation (3.5) allows us to define a velocity potential, ϕ, as follows:

$$\mathbf{u} = \nabla\phi \tag{3.8}$$

By using this we can now write equation (3.3) as Laplace's equation:

$$\nabla^2\phi = 0 \tag{3.9}$$

Now only an equation for the pressure remains, and we obtain this by integrating the vertical component of equation (3.6) with respect to y and apply equation (3.8):

$$\frac{p - p_0}{\rho} = B(t) - \phi_t - \frac{1}{2}(\nabla\phi)^2 - gy$$

where $B(t)$ is an arbitrary function coming from the integration, and the constant p_0 is separated from $B(t)$.

If we define a new potential as $\phi' = \phi - \int B(t)dt$, we absorb the function $B(t)$ into ϕ' and get the Bernoulli equation (we assume this was done from the beginning and drop the primed notation for ϕ):

$$\frac{p - p_0}{\rho} = -\phi_t - \frac{1}{2}(\nabla\phi)^2 - gy \tag{3.10}$$

This equation balances the work done on the fluid by the pressure forces with the change in kinetic energy of the flow.

3.2 Boundary conditions

In this section three boundary conditions will be given, two for the free surface and one for the bottom. At the end the full free surface problem will be stated.

We start with the dynamic surface condition, which states that the forces in the 'fluids' on the two sides of the massless interface must be equal at the interface. Since we neglect surface tension this is the same as saying that the pressure in the water and the pressure in the air must be equal at the surface. We do this by letting $p = p_0$ in equation (3.10) and evaluate at the surface:

$$\phi_t + \frac{1}{2}(\phi_x^2 + \phi_y^2) + g\eta = 0 \text{ on } y = \eta(x, t) \tag{3.11}$$

We also have the kinematic surface condition, which states that the velocity of the fluid normal to the interface must be equal to the velocity of the interface normal to itself:

$$\frac{D\eta}{Dt} = \eta_t + u\eta_x = v \text{ on } y = \eta(x, t) \tag{3.12}$$

A more intuitive way of looking at this is to say that fluid particles in the surface will remain in the surface.

The bottom of the canal is a solid fixed boundary, so we have here that the normal velocity of the fluid must vanish. If we define $\mathbf{n}$ to be the normal vector at the bottom pointing upwards, we get:

$$\mathbf{n} \cdot \nabla\phi = 0 \text{ on } y = -h_0$$

which, due to the fact that the bottom is flat, can be written more conveniently as:

$$\phi_y = 0 \text{ on } y = -h_0 \tag{3.13}$$

To summarize, the full free surface problem in two spatial dimensions is given by:

$$\begin{aligned} \phi_{xx} + \phi_{yy} &= 0 \quad \text{on} \quad -h_0 < y < h_0 + \eta \\ \eta_t + \phi_x\eta_x - \phi_y &= 0 \quad \text{on } y = \eta \\ \phi_t + \frac{1}{2}(\phi_x^2 + \phi_y^2) + g\eta &= 0 \quad \text{on } y = \eta \\ \phi_y &= 0 \quad \text{on } y = -h_0 \end{aligned} \tag{3.14}$$

Both the shallow water and Boussinesq system of equations can be derived as limiting cases of this.

3.3 The linearized theory

In this section the linearized water wave equations will be derived, starting with the system (3.14). Since this will be a linear problem in η and ϕ it can be solved by guessing elementary sinusoidal solutions of η. We then go on to derive expressions for the horizontal and vertical velocity components, in addition to the dispersion relation. We can then also give expressions for the phase speed and the group speed. The following derivation can also be found in [6].

We start by assuming only small perturbations of the free surface and that both the horizontal and vertical components of the velocity field are small quantities. We assume in addition that they are of the same order of magnitude, and write $u, v, \eta \sim O(\epsilon)$ such that all terms of $O(\epsilon^2)$ are small enough to be neglected.

We begin the derivation by disregarding the nonlinear term in the kinematic boundary condition at the free surface, equation (3.12), since this is of $O(\epsilon^2)$, and get:

$$\frac{\partial \eta}{\partial t} = \frac{\partial \phi}{\partial y} \quad \text{on} \quad y = \eta(x,t)$$

we continue by expanding the term on the right about the equilibrium level of the surface:

$$\left.\frac{\partial \phi}{\partial y}\right|_{y=\eta} = \left.\frac{\partial \phi}{\partial y}\right|_{y=0} + \eta \left.\frac{\partial \phi}{\partial y}\right|_{y=0} + \cdots$$

truncate this expression after the first term such that the error is of $O(\epsilon^2)$, and get the linearized formulation of the kinematic surface condition:

$$\frac{\partial \eta}{\partial t} = \frac{\partial \phi}{\partial y} \quad \text{on} \quad y = 0 \tag{3.15}$$

For the dynamic boundary condition at the fee surface, (3.11), we proceed in a similar way, by disregarding the nonlinear terms to get the following:

$$\frac{\partial \phi}{\partial t} + g\eta = 0 \quad \text{on} \quad y = \eta(x,t)$$

We may then expand $\frac{\partial \phi}{\partial t}|_{y=\eta}$ about $y = 0$, keep only the first term such that the error again is of $O(\epsilon^2)$, and get the linearized dynamic surface condition:

$$\frac{\partial \phi}{\partial t} + g\eta = 0 \quad \text{on} \quad y = 0 \tag{3.16}$$

By differentiating this equation with respect to time we can use the linearized kinematic surface condition, equation (3.15), to eliminate η as follows:

$$\phi_{tt} + g\phi_y = 0 \quad \text{on} \quad y = 0 \tag{3.17}$$

The boundary condition at the bottom is already linear and independent of η, thus we now have the system (3.14) as a linear problem, with ϕ as the only dependent variable:

$$\begin{aligned} \phi_{xx} + \phi_{yy} &= 0 \quad \text{on} \quad -h_0 < y < 0 \\ \phi_{tt} + g\phi_y &= 0 \quad \text{on} \quad y = 0 \\ \phi_y &= 0 \quad \text{on} \quad y = -h_0 \end{aligned} \tag{3.18}$$

This system models linear waves of small amplitude on water initially at rest where the bottom is of constant depth. We therefore assume the following form for η:

$$\eta(x,t) = a_0 \cos(kx - \omega t) \tag{3.19}$$

where the amplitude, a_0, is of $O(\epsilon)$.

From the linearized surface conditions, equations (3.15) and (3.16), and by applying separation of variables, we now get the following expression for ϕ:

$$\phi(x,y,t) = f(y)\sin(kx - \omega t) \tag{3.20}$$

After inserting this into the Laplace equation we see that this form of ϕ is a solution provided:

$$\frac{d^2 f}{dy^2} - f(y)k^2 = 0$$

This is a standard second order ODE and the general solution is given by:

$$f(y) = Ae^{ky} + Be^{-ky}$$

Thus equation (3.20) takes the form:

$$\phi(x,y,t) = (Ae^{ky} + Be^{-ky})\sin(kx - \omega t) \tag{3.21}$$

The values of the constants A and B can be found by inserting this expression into the boundary conditions.

From the condition at the bottom, (3.13), we get the following:

$$\left.\frac{\partial \phi}{\partial y}\right|_{y=-h_0} = (kAe^{-kh_0} - kBe^{kh_0})\sin(kx - \omega t) = 0 \implies B = Ae^{-2kh_0}$$

and from the kinematic surface condition, (3.15), we get:

$$\left.\frac{\partial \phi}{\partial y}\right|_{y=0} = k(A - B)\sin(kx - \omega t) = \frac{\partial \eta}{\partial t} \implies k(A - B) = a_0\omega$$

We now have two equations involving the constants A and B, which can be solved to obtain:

$$A = \frac{a_0\omega}{k(1 - e^{-2kh_0})} \quad \text{and} \quad B = \frac{a_0\omega e^{-2kh_0}}{k(1 - e^{-2kh_0})}$$

After substituting this into equation (3.21) we get the full expression for ϕ:

$$\phi(x,y,t) = \frac{a_0\omega}{k}\frac{\cosh(k(y+h_0))}{\sinh(kh_0)}\sin(kx-\omega t) \tag{3.22}$$

The horizontal and vertical velocity components are now obtained by differentiating ϕ with respect to x and y, respectively:

$$\begin{aligned} u = \phi_x &= a_0\omega\frac{\cosh(k(y+h_0))}{\sinh(kh_0)}\cos(kx-\omega t) \\ v = \phi_y &= a_0\omega\frac{\sinh(k(y+h_0))}{\sinh(kh_0)}\sin(kx-\omega t) \end{aligned} \tag{3.23}$$

We used only the boundary condition at the bottom and the kinematic surface condition to obtain (3.22), thus substituting ϕ into the dynamic surface condition, equation (3.16), yields additional information, namely the dispersion relation:

$$\begin{aligned} -\frac{a_0\omega^2}{k}\frac{\cosh(kh_0)}{\sinh(kh_0}\cos(kx-\omega t) &= -ga_0\cos(kx-\omega t) \\ \implies \omega^2 &= gk\tanh(kh_0) \end{aligned} \tag{3.24}$$

Solving (3.24) for ω yields two modes of opposite signs, and they represent waves propagating to the left (minus sign for negative x-direction) and to the right (plus sign for positive x-direction), respectively.

The figure below shows the positive mode of ω as a function of k, when the constants g and h_0 are set to unity. The negative mode is identical, only mirrored over the horizontal axis.

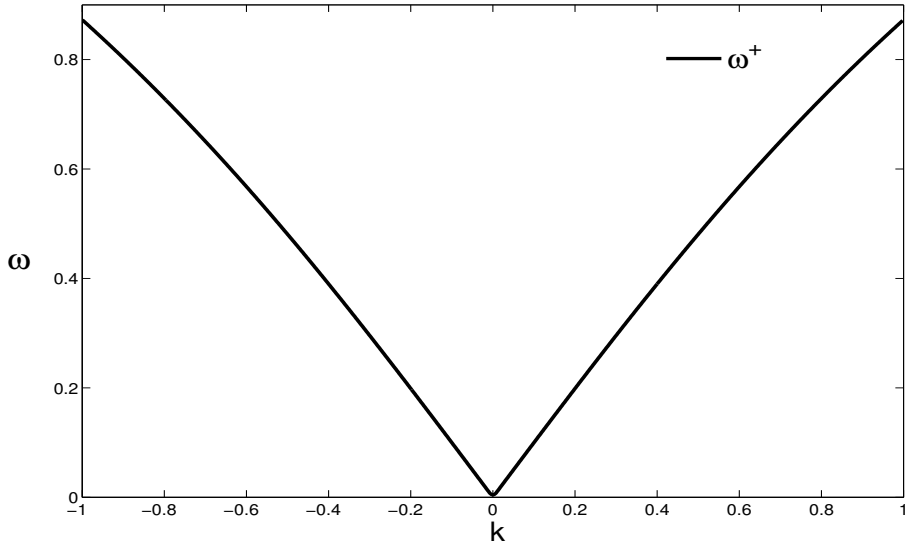

Figure 3.1: Linear dispersion relation

Since we now have the dispersion relation, we can also find the phase and group speeds:

$$\begin{aligned} c_p &= \frac{\omega}{k} = \pm g \tanh(kh_0) \\ c_g &= \frac{\partial \omega}{\partial k} = \pm \frac{1}{2} c_p \left(1 + \frac{2kh_0}{\sinh(2kh_0)} \right) \end{aligned} \tag{3.25}$$

where the different signs again denote horizontal direction.

3.4 Shallow water theory

To get a first look at waves in shallow water (or equivalently waves of long wavelength) we assume $kh_0 \ll 1$, which is the same as saying that wavelength is much larger than water depth.

For small values of the argument we have that $\tanh(x) \approx x$, $\sinh(x) \approx x$ and $\cosh(x) \approx 1$, and we use this to obtain a limiting shallow water/long waves approximation of the linearized theory.

We begin by applying this to the dispersion relation, equation (3.24), which then takes the form:

$$\omega^2 = c_0^2 k^2 \tag{3.26}$$

where $c_0 = \sqrt{gh_0}$ is the limiting long wave/shallow water phase speed (this is seen immediately from $c_p = \frac{\omega}{k}$). In this case ω is proportional to k and there is no dispersion at all (i.e. $c_p = c_g = c_0$).

Under the same reasoning the horizontal and vertical velocity components, (3.23), become:

$$u = \phi_x = \frac{\omega a_0}{k h_0} \cos(kx - \omega t) = c_0 \frac{\eta}{h_0}$$
$$v = \phi_y = \omega a_0 (1 + \frac{y}{h_0}) \sin(kx - \omega t)$$

From here we can see that the horizontal velocity component is in fact independent of the vertical coordinate.

Now that we have some idea of how waves on shallow water behave, we can continue by incorporating some nonlinear effects. The following derivation can also be found in chapter 13 of [1].

The first step is to neglect the vertical acceleration in the vertical component of the momentum equation, (3.1), which then takes the form:

$$-\frac{\partial p}{\partial y} - \rho g = 0 \tag{3.27}$$

and integrate it vertically as follows:

$$\int_p^{p_0} dp = -\rho g \int_y^{\eta} dy \implies p - p_0 = \rho g (\eta - y) \tag{3.28}$$

By using this, the horizontal component of the momentum equation can be written as:

$$\frac{\partial u}{\partial t} + u\frac{\partial u}{\partial x} + v\frac{\partial u}{\partial y} = -g\frac{\partial \eta}{\partial x}$$

Since the right hand side is independent of y, the material derivative of the horizontal velocity component must also be independent of y, and we can write:

$$\frac{\partial u}{\partial t} + u\frac{\partial u}{\partial x} + g\frac{\partial \eta}{\partial x} = 0 \tag{3.29}$$

We continue by integrating the equation for conservation of mass, equation (3.3), over the total depth as follows:

$$0 = \int_{-h_0}^{\eta} \frac{\partial u}{\partial x} + \frac{\partial v}{\partial y} dy = \frac{\partial}{\partial x} \int_{-h_0}^{\eta} u dy + [v]_{y=-h_0}^{y=\eta} - u|_{y=\eta} \frac{\partial \eta}{\partial x}$$

where the last term on the right hand side comes from the fact that η is dependent of x while h_0 is a constant.

Now we can use the kinematic boundary condition at the surface, (3.12), along with the boundary condition at the bottom, (3.13), to substitute for the two terms involving the vertical velocity component, in which case the integrated mass conservation equation reduces to:

$$\frac{\partial}{\partial x}\int_{-h_0}^{\eta} u dy + \frac{\partial \eta}{\partial t} = 0$$

Since we previously stated that the horizontal velocity component is independent of depth, this equation can be written as:

$$\frac{\partial \eta}{\partial t} + \frac{\partial}{\partial x}[u(\eta + h_0)] = 0 \tag{3.30}$$

This is in the form of a conservation equation, which comes as no surprise, since it was derived by integrating equation (3.3).

Equations (3.29) and (3.30) provide a nonlinear set for waves on shallow water, or equivalently waves of long wavelength. By linearizing these equations we should obtain the dispersion relation (3.26), so we continue by checking this. Linearizing (3.29) and (3.30) yields:

$$\eta_t + h_0 u_x = 0$$
$$u_t + g\eta_x = 0$$

and by differentiating the first of these with respect to t, and the second with respect to x, combining the two to eliminate u yields the one dimensional wave equation in terms of η:

$$\eta_{tt} - c_0^2 \eta_{xx} = 0 \tag{3.31}$$

Upon substituting equation (3.19) for η, and solving for ω we do in fact obtain the dispersion relation (3.26).

We can estimate the error of the nonlinear system, (3.29) and (3.30), by a few simple scaling arguments. In obtaining (3.28) the error is of order $\rho h_0 v_t$, and from equation (3.3) we have that $v \approx -h_0 u_x$. Thus, the relative error in equation (3.29) is of the order:

$$-\frac{p_x}{\rho u_t} \approx \frac{h_0^2 u_{xxt}}{u_t} \approx \frac{h_0^2}{l^2} \tag{3.32}$$

This fits well with the estimates done previously in this section with the linearized equations, where we assumed $kh_0 \ll 1$.

We have already seen that the linearized shallow water equations does not include dispersive effects, so to see if the nonlinear ones do, we approximate the $\tanh(\cdot)$ factor in (3.24) more precisely by doing a formal expansion:

$$\tanh(kh_0) = kh_0 - \frac{(kh_0)^3}{3} + \frac{2(kh_0)^5}{15} - ...$$

Keeping the two first terms gives (3.24) as:

$$\omega^2 = c_0^2 k^2 - \frac{1}{3} c_0^2 h_0^2 k^4 \tag{3.33}$$

Thus, there is no dispersive effects in equations (3.29) and (3.30), as the second term in the dispersion relation is of a higher order in $\frac{h_0^2}{l^2}$. This means there is nothing to balance the nonlinear effects, and all waves carrying an increase of elevation will eventually break [1].

The goal of the next section is to include dispersive effects in the shallow water theory such that the linearized version of those equations yield the dispersion relation (3.33). Including too much of the dispersive effects, however, will result in no waves breaking.

3.5 The Boussinesq approximation

In this section the normalized Boussinesq equations will be derived. These equations are valid for weakly non-linear and fairly long/shallow water waves. This is part of the Boussinesq approximation, whose goal is to eliminate the vertical coordinate from the flow equations while at the same time retaining some of the vertical structure of the flow. This can be done because the waves propagate in the horizontal direction, while having a different, not wave-like, behavior in the vertical direction.

The steps in the approximation are as follows:
- the horizontal velocity field is expanded around a certain depth
- vertical partial derivatives are replaced with horizontal partial derivatives
- the expansion is truncated to a finite number of terms such that both some non-linear and dispersive effects are retained
- the vertical dependence of the flow equations are eliminated

The resulting system should contain only two dependent variables, namely the deformation of the free surface and the horizontal velocity field evaluated at a certain depth in the water column.

We start by introducing a new independent variable, Y, which will be measured vertically from the bottom of the canal ($Y = 0$ at the bottom and $Y = h_0$ at the equilibrium level of the surface). In this new reference system, where position is given by the coordinates (x, Y), equation (3.9) now looks like:

$$\phi_{xx} + \phi_{YY} = 0 \tag{3.34}$$

with $\phi_Y = 0$ on $Y = 0$ (analogous to (3.13)).

We continue by expanding the velocity potential around a certain elevation (here $Y = 0$ is chosen for convenience):

$$\phi = \phi\Big|_{Y=0} + Y\frac{\partial\phi}{\partial Y}\Big|_{Y=0} + \frac{Y^2}{2}\frac{\partial^2\phi}{\partial Y^2}\Big|_{Y=0} + \cdots = \sum_{n=0}^{\infty} Y^n f_n(x,t)$$

where $f_0 = \phi|_{Y=0}$.

If we use equation (3.34) along with the boundary condition at $Y = 0$ we can drop every other term and the expansion can be written as:

$$\phi = \phi\Big|_{Y=0} - \frac{Y^2}{2}\frac{\partial^2\phi}{\partial x^2}\Big|_{Y=0} + \frac{Y^4}{24}\frac{\partial^4\phi}{\partial x^4}\Big|_{Y=0} + \cdots = \sum_{n=0}^{\infty}(-1)^n\frac{Y^{2n}}{(2n)!}\frac{\partial^{2n} f}{\partial x^{2n}} \tag{3.35}$$

where $f = f_0$.

Before this expression can be inserted into the boundary conditions at the free surface, we normalize the variables as follows (original variables are primed):

$$x' = lx,\ Y' = h_0 Y,\ t' = \frac{lt}{c_0},\ \eta' = a_0\eta,\ \phi' = \frac{gla_0\phi}{c_0} \tag{3.36}$$

In addition we define the dimensionless parameters α and β:

$$\alpha = \frac{a_0}{h_0},\ \beta = \frac{h_0^2}{l^2} \tag{3.37}$$

where α represents the relative amplitude and β the relative wavenumber. The waves fall into the Boussinesq regime if α and β are both small and of the

same order of magnitude, so we assume this to be the case. α and β can also be seen as to represent nonlinear effects and dispersive effects, respectively. In later sections α will denote bore strength, as stated in the introduction. These parameters become very useful when substituting the expansion for ϕ into the surface conditions, because then the terms can be ordered in powers of α and β, and the higher order terms can easily be identified. In contrast to the previous section we now keep terms of $O(\beta)$.

In these new normalized variables equations (3.14) can be written as:

$$\begin{aligned} \beta\phi_{xx} + \phi_{YY} &= 0 \text{ on } 0 < Y < 1 + \alpha\eta \\ \eta_t + \alpha\phi_x\eta_x - \frac{1}{\beta}\phi_Y &= 0 \text{ on } Y = 1 + \alpha\eta \\ \eta + \phi_t + \frac{1}{2}\alpha\phi_x^2 + \frac{1}{2}\frac{\alpha}{\beta}\phi_Y^2 &= 0 \text{ on } Y = 1 + \alpha\eta \\ \phi_Y &= 0 \text{ on } Y = 0 \end{aligned} \tag{3.38}$$

and the expansion for ϕ, equation (3.35), now appears in powers of β:

$$\phi = \sum_{n=0}^{\infty}(-1)^n \frac{Y^{2n}}{(2n)!}\frac{\partial^{2n} f}{\partial x^{2n}}\beta^n \tag{3.39}$$

By substituting this expression into the normalized kinematic and dynamic surface conditions in (3.38), respectively, and drop all terms of $O(\beta^2)$, we obtain:

$$\eta_t + \{(1+\alpha\eta)f_x\}_x - \{\frac{1}{6}(1+\alpha\eta)^3 f_{xxxx} + \frac{1}{2}\alpha(1+\alpha\eta)^2\eta_x f_{xxx}\}\beta + O(\beta^2) = 0$$

$$\eta + f_t + \frac{1}{2}\alpha f_x^2 - \frac{1}{2}(1+\alpha\eta)^2\{f_{xxt} + \alpha f_x f_{xxx} - \alpha f_{xx}^2\}\beta + O(\beta^2) = 0$$

If we differentiate the second of these equations with respect to x and keep $O(\beta)$ - terms but drop all terms of $O(\alpha\beta)$, we get one variant of the normalized Boussinesq equations:

$$\begin{aligned} \eta_t + \{(1+\alpha\eta)w\}_x - \frac{1}{6}\beta w_{xxx} + O(\alpha\beta, \beta^2) &= 0 \\ w_t + \alpha w w_x + \eta_x - \frac{1}{2}\beta w_{xxt} + O(\alpha\beta, \beta^2) &= 0 \end{aligned} \tag{3.40}$$

where $w = f_x = \frac{\partial \phi}{\partial x}|_{Y=0}$ is the first term in the expansion of the horizontal velocity:

$$u = \phi_x = w - \beta \frac{Y^2}{2} w_{xx} + O(\beta^2) \tag{3.41}$$

Similarly, the vertical velocity appear now as:

$$v = \phi_Y = -\beta Y w_x + O(\beta^2) \tag{3.42}$$

If we average equation (3.41) over the depth of the canal we obtain:

$$\tilde{u} = \frac{1}{1+\alpha\eta} \int_0^{1+\alpha\eta} \left(w - \beta \frac{Y^2}{2} w_{xx} + O(\beta^2) \right) dY = \left(1 - \frac{1}{6} \beta \frac{\partial^2}{\partial x^2} \right) w + O(\alpha\beta, \beta^2)$$

and by taking the inverse we get:

$$\begin{aligned} w &= \frac{1}{1 - \frac{\beta}{6}\frac{\partial^2}{\partial x^2}} \tilde{u} = \left(1 + \frac{\beta}{6} \frac{\partial^2}{\partial x^2} + \cdots \right) \tilde{u} \\ \Longrightarrow w &= \tilde{u} + \frac{1}{6} \beta \tilde{u}_{xx} + O(\alpha\beta, \beta^2) \end{aligned}$$

Substituting for w in equations (3.40) now yields:

$$\begin{aligned} \eta_t + \{(1+\alpha\eta)\tilde{u}\}_x + O(\alpha\beta, \beta^2) = 0 \\ \tilde{u}_t + \alpha \tilde{u} \tilde{u}_x + \eta_x - \frac{1}{3} \beta \tilde{u}_{xxt} + O(\alpha\beta, \beta^2) = 0 \end{aligned} \tag{3.43}$$

If we solve the first of these equations for $\tilde{u}_x$ to the lowest order we get:

$$\tilde{u}_x = -\eta_t + O(\alpha, \beta)$$

and by differentiating this with respect to both x and t we can substitute for the $\tilde{u}_{xxt}$ - term in the second of equations (3.43) as follows:

$$\frac{1}{3} \beta \tilde{u}_{xxt} = \frac{1}{3} \beta \eta_{ttx} + O(\alpha\beta, \beta^2)$$

The result is the normalized Boussinesq equations (order term is dropped):

$$\begin{aligned} \eta_t + \{(1+\alpha\eta)\tilde{u}\}_x &= 0 \\ \tilde{u}_t + \alpha\tilde{u}\tilde{u}_x + \eta_x + \frac{1}{3}\beta\eta_{xtt} &= 0 \end{aligned} \tag{3.44}$$

Note: if we also were to drop all terms of $O(\beta)$ in (3.40) we would get the normalized form of the nonlinear shallow water equations, (3.29) and (3.30):

$$\begin{aligned} \eta_t + \{(1+\alpha\eta)w\}_x &= 0 \\ w_t + \alpha w w_x + \eta_x &= 0 \end{aligned}$$

3.6 The Korteweg-deVries equation

In this section the Korteweg-deVries equation will be derived.

The KdV equation was first derived by Boussinesq in 1877, but this had little impact as it only appeared as a footnote in his "Essai sur la theorie des eaux courantes" [11]. Independently of this, it was later derived again in 1895 by Diederik Korteweg and Gustav deVries [13]. In the context of water waves, the KdV equation models one dimensional weakly nonlinear dispersive waves at the surface of a shallow body of water.

Although solutions of the KdV equation describe the free surface of the fluid, the underlying vertical structure of the flow is still encoded into the equation, just as with the Boussinesq system derived in the previous section. While the Boussinesq equations allow for waves to propagate in opposing directions simultaneously, we shall derive the KdV equation from the Boussinesq system simply by specializing to a wave traveling to the right. The assumptions of small amplitude and long wavelength compared to the undisturbed depth of the fluid is still in place, as the KdV equation fall under the Boussinesq parameter regime.

If we drop all terms of $O(\alpha, \beta)$ in equations (3.40) we get the system:

$$\begin{aligned} \eta_t + w_x + O(\alpha,\beta) &= 0 \\ w_t + \eta_x + O(\alpha,\beta) &= 0 \end{aligned}$$

This system can be solved exactly, yielding one right going solution and one left going solution. We are only interested in the right going solution, which gives the relations:

$$w = \eta \text{ and } \eta_t + \eta_x = 0 \tag{3.45}$$

Thus, we look for a solution of (3.40) in the form:

$$w = \eta + \alpha A + \beta B + O(\alpha^2 + \beta^2) \tag{3.46}$$

where A and B are functions of η and its x - derivatives.

To find explicit expressions for A and B we insert this solution into equations (3.40):

$$\begin{aligned} \eta_t + \eta_x + \alpha(A_x + 2\eta\eta_x) + \beta\left(B_x - \frac{1}{6}\eta_{xxx}\right) + O(\alpha^2 + \beta^2) = 0 \\ \eta_t + \eta_x + \alpha(A_t + \eta\eta_x) + \beta\left(B_t - \frac{1}{2}\eta_{xxt}\right) + O(\alpha^2 + \beta^2) = 0 \end{aligned} \tag{3.47}$$

Since we know from (3.45) that $\eta_t = -\eta_x + O(\alpha, \beta)$, we can replace all t - derivatives in these equations by minus the x - derivatives. The two equations will then be consistent if $A = -\frac{1}{4}\eta^2$ and $B = \frac{1}{3}\eta_{xx}$.

By inserting this into the second of equations (3.47) we get the normalized KdV equation (the order term is dropped):

$$\eta_t + \eta_x + \frac{3}{2}\alpha\eta\eta_x + \frac{1}{6}\beta\eta_{xxx} = 0$$

Now that we have derived the KdV equation we can revert back to the original variables:

$$\eta_t + c_0\eta_x + \frac{3}{2}\frac{c_0}{h_0}\eta\eta_x + \frac{1}{6}c_0h_0^2\eta_{xxx} = 0$$

The linearized form of this equation should give the dispersion relation (3.33), so we check this by inserting (3.19) into:

$$\eta_t + c_0\eta_x + \frac{1}{6}c_0h_0^2\eta_{xxx} = 0$$

which gives:

$$\omega = c_0k - \frac{1}{6}c_0h_0^2k^3$$

Equation (3.33) can be written as:

$$\omega = k\sqrt{gh_0(1 - \frac{(kh_0)^2}{3})}$$

and if we in addition apply the series expansion $\sqrt{1+x} = 1 + \frac{1}{2}x - \frac{1}{2}x^2 + \cdots$ on the square root we can write:

$$\omega = c_0 k - \frac{1}{6} c_0 h_0^2 k^3$$

Thus, we succeeded in incorporating dispersive effects in the shallow water theory.

From here on we set $g = 1$ and $h_0 = 1$, such that the KdV equation takes the form:

$$\eta_t + \eta_x + \frac{3}{2}\eta\eta_x + \frac{1}{6}\eta_{xxx} = 0 \tag{3.48}$$

In other words, h_0 represents a unit of distance, and $\sqrt{h_0/g}$ represents a unit of time. In the remainder of this report it is this form of the KdV equation that will be used.

Note: It is worth mentioning that the KdV equation also frequently appears in the following form:

$$\eta_t + 6\eta\eta_x + \eta_{xxx} = 0$$

This can be obtained from equation (3.48) by the transformation:

$$t' = \frac{1}{6}t, \quad x' = x - t \quad \text{and} \quad \eta' = \frac{3}{2}\eta$$

Chapter 4

Traveling wave solutions of the KdV equation

One of the advantages of the KdV equation is that it can be solved exactly, which is rare for a nonlinear partial differential equation. This is probably one of the reasons why it has been studied so extensively. The KdV equation allows for both solitary wave solutions and periodic wave solutions, both of which can be found explicitly, although the solitary wave is far more easy to obtain.

In this chapter we shall start by deriving the solitary wave solution, and then the more general periodic solution. Due to the use of Jacobian elliptic functions in describing the periodic solution, the term 'cnoidal wave' is frequently used in the literature on the subject. It shall also be seen that the solitary wave solution in fact is a limiting case of the cnoidal solution. The following can also be found in [4], [18] and [1].

4.1 The solitary wave

Both the solitary waves and the periodic waves described by the KdV equation, (3.48), are found as solutions moving with constant shape and constant velocity. We may therefore describe them as:

$$\eta(x,t) = f(\zeta) \text{ where } \zeta = x - ct \tag{4.1}$$

By inserting this into (3.48) we obtain:

$$(1-c)f' + \frac{3}{2}ff' + \frac{1}{6}f''' = 0$$

After integration this leads to:

$$(1-c)f + \frac{3}{4}f^2 + \frac{1}{6}f'' = \frac{1}{4}A$$

Where A is an integration constant. Further, we multiply with $4f'$ and integrate once more to obtain:

$$2(1-c)f^2 + f^3 + \frac{1}{3}(f')^2 = Af + B \tag{4.2}$$

Where B is a constant coming from the second integration.

From the definition of a solitary wave we have that f and its derivatives must tend to zero as ζ tends to $\pm\infty$. So by letting $f, f', f'' \to 0$ we immediately see that $A = 0$ and $B = 0$. By doing this equation (4.2) now looks like:

$$(\frac{df}{d\zeta})^2 = (f)^2(6(c-1) - 3f)$$

Since $\frac{df}{d\zeta}$ must be real valued we have that $(6(c-1) - 3f) \geq 0$, although $\frac{df}{d\zeta} = 0$ only leads to trivial solutions.

We have now transformed the KdV equation into an ordinary differential equation which can be solved by evaluating the following integrals:

$$\int \frac{df}{f\sqrt{6(c-1) - 3f}} = \pm \int d\zeta \tag{4.3}$$

By using the substitution $f = 2(c-1)\,\mathrm{sech}^2(\theta)$ we transform the first of these as follows:

$$\frac{2}{\sqrt{6(c-1)}} \int d\theta = \mp \int d\zeta$$

The solution is now easily obtained:

$$f(x-ct) = \eta(x,t) = H\,\mathrm{sech}^2\left(\frac{\sqrt{3H}}{2}(x - ct - x_0)\right) \tag{4.4}$$

where x_0 is a constant coming from the last integration, and the phase speed, c, is given by:

$$c = \frac{H}{2} + 1 \tag{4.5}$$

Equation (4.4) is the solitary wave solution of the KdV equation. The nonlinearity of the solitary wave is apparent from the fact that the propagation speed, c is dependent on the wave height, H.

The figure below shows the solitary wave in one instant in time for $H = 0.1$:

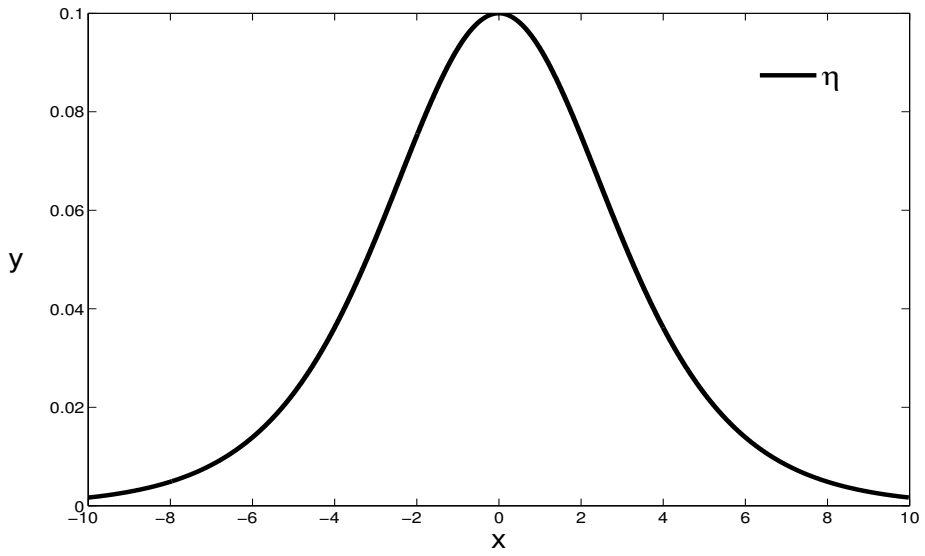

Figure 4.1: Solitary wave

Note: The $\pm$ in equation (4.3) is redundant since (4.4) is an even function. The constant x_0 denotes the phase shift and can easily be ignored.

4.2 The cnoidal wave

To derive the cnoidal wave we start with equation (4.2) which, for arbitrary A and B can be written as:

$$\frac{1}{3}(f')^2 = -f^3 + 2(c-1)f^2 + Af + B = F(f) \tag{4.6}$$

where, as before, a real solution will only exist in regions where $F(f) \geq 0$.

Since $F(f)$ is a third order polynomial in f we know that $F(f)$ must have at least one real zero. If F only has one real zero, then the other two must be a complex conjugate pair, and there will only be one value of f for which F and thus also f' vanishes. However, since we are looking for a periodic solution, there must be both crests and troughs (i.e. points where f' vanishes), and therefore more than just one value of f for which f' vanishes. We conclude that all three zeros of F must be real.

Three cases now naturally arise:
i) $F(f)$ has a triple zero
ii) $F(f)$ has a double zero
iii) $F(f)$ has only single zeros

Assume *i*) is the case, and let $f = f_0$ be a triple zero of F. Then we can write: $F(f) = -(f - f_0)^3$, and from equation (4.6) we see that the only possibility is: $f_0 = \frac{2}{3}(c-1)$.

The solution is then easily obtained as:

$$f(\zeta) = \frac{2}{3}(c-1) - \frac{4}{3(\zeta - x_0)^2}$$

Where x_0 is a constant of integration. This solution becomes unbounded as ζ approaches x_0 and is therefore not relevant.

If *ii*) is the case, a real solution will either be unbounded as in *i*), or the solution will be the solitary wave discussed earlier. Thus *iii*) is the only relevant case.

Let these three distinct real zeros be denoted by $f_1 = f(\zeta_1)$, $f_2 = f(\zeta_2)$ and $f_3 = f(\zeta_3)$, where $f_3 < f_2 < f_1$. Then, by the form of F, a real and bounded solution will exist in the finite interval between f_2 and f_1, and will

oscillate between the two points with a finite period.

The figure below shows F as a function of f when iii) is the case. The dotted line represents $F = 0$.

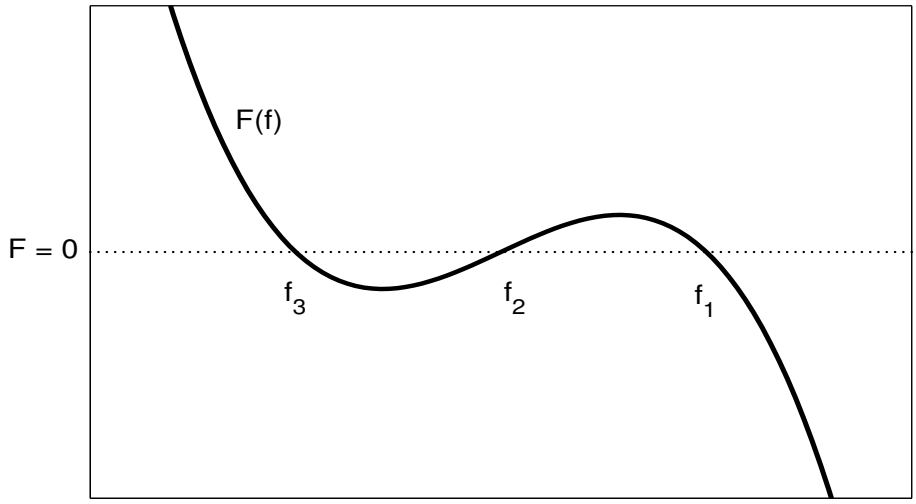

Figure 4.2: Zeros of $F(f)$

We thus assume the right hand side of equation (4.6) can be written as:

$$F(f) = -(f - f_1)(f - f_2)(f - f_3) \tag{4.7}$$

where $f_2 \leq f \leq f_1$. In other words, f_1 denotes the crest elevation, and f_2 denotes the trough elevation (measured from the equilibrium level of the surface). A periodic function satisfying this range of oscillation can be represented as:

$$f(\zeta) = f_1 \cos^2 \psi(\zeta) + f_2 \sin^2 \psi(\zeta) \tag{4.8}$$

where the unknown function $\psi(\zeta)$ gives the phase.

Since we have that $f(\zeta_1) = f_1$, we get from this that $\psi(\zeta_1) = 0, 2\pi, \cdots$ and similarly, since $f(\zeta_2) = f_2$, we get $\psi(\zeta_2) = \pi/2, 3\pi/2, \cdots$. Thus the distance from the peak to the trough in terms of ψ is: $\pi/2$.

Also using equation (4.8), we can obtain the following expressions:

$$\begin{aligned} f - f_1 &= f_1(\cos^2\psi(\zeta) - 1) + f_2\sin^2\psi(\zeta) = -(f_1 - f_2)\sin^2\psi(\zeta) \\ f - f_2 &= f_1\cos^2\psi(\zeta) + f_2(\sin^2\psi(\zeta) - 1) = (f_1 - f_2)\cos^2\psi(\zeta) \\ f - f_3 &= -(f_1 - f_2)\sin^2\psi(\zeta) + (f_1 - f_3) \\ f' &= -2(f_1 - f_2)\sin\psi(\zeta)\cos\psi(\zeta)\frac{d\psi}{d\zeta} \end{aligned} \tag{4.9}$$

These can now be inserted into equation (4.6), using also equation (4.7), to obtain an ordinary differential equation in terms of $\psi(\zeta)$:

$$\frac{4}{3}(\frac{d\psi}{d\zeta})^2 = (f_1 - f_3) - (f_1 - f_2)\sin^2\psi(\zeta) \tag{4.10}$$

Since $(f_1 - f_3) > (f_1 - f_2)$ the right hand side is positive, and ensures a real solution for ψ.

In addition we know that $F(f)$ has no zeros in the interval $f_2 < f < f_1$, and thus we may assume ψ to be a monotone function. This allows us to transform the above expression into an ordinary differential equation in terms of $\zeta(\psi)$:

$$\frac{\sqrt{3(f_1 - f_3)}}{2}\frac{d\zeta}{d\psi} = \pm\frac{1}{\sqrt{1 - m\sin^2\psi}} \tag{4.11}$$

where $m = (f_1 - f_2)/(f_1 - f_3)$, such that $0 < m < 1$.

We may now integrate equation (4.11) to obtain the solution implicitly:

$$\frac{\sqrt{3(f_1 - f_3)}}{2}\int_{\zeta_1}^{\zeta} d\tilde{\zeta} = \pm\int_{\psi(\zeta_1)=0}^{\psi}\frac{d\tilde{\psi}}{\sqrt{1 - m\sin^2\tilde{\psi}}} \tag{4.12}$$

The integral on the right hand side is now the incomplete elliptic integral of the first kind, with elliptic parameter m. This is defined by:

$$u = \int_0^{\phi}\frac{d\theta}{\sqrt{1 - m\sin^2\theta}}$$

The elliptic functions $\mathrm{sn}(\cdot|m)$, $\mathrm{cn}(\cdot|m)$ and $\mathrm{dn}(\cdot|m)$ are defined as inverses of this:

$$\begin{aligned}\mathrm{sn}(u|m) &= \sin\phi \\ \mathrm{cn}(u|m) &= \cos\phi \\ \mathrm{dn}(u|m) &= \sqrt{1 - m\sin^2\phi}\end{aligned}$$

where the following algebraic relations between them holds:

$$\mathrm{sn}^2(u|m) + \mathrm{cn}^2(u|m) = 1 \quad \text{and} \quad \mathrm{dn}^2(u|m) + m^2\,\mathrm{sn}^2(u|m) = 1$$

Elliptic integrals are said to be complete when $\phi = \pi/2$, and so the complete elliptic integrals of the first and second kind, respectively, are defined by:

$$K(m) = \int_0^{\pi/2} \frac{d\theta}{\sqrt{1 - m\sin^2\theta}} \quad \text{and} \quad E(m) = \int_0^{\pi/2} \sqrt{1 - m\sin^2\theta}\; d\theta$$

By applying this to (4.12) we get:

$$\mathrm{sn}\left(\frac{\zeta - \zeta_1}{\sigma}|m\right) = \sin\psi \quad \text{and} \quad \mathrm{cn}\left(\frac{\zeta - \zeta_1}{\sigma}|m\right) = \cos\psi \tag{4.13}$$

Where $\sigma^2 = \frac{4}{3(f_1 - f_3)}$.

We can now apply equation (4.8) to obtain the following:

$$\begin{aligned} f(\zeta) &= f_2 + (f_1 - f_2)\,\mathrm{cn}^2\left(\frac{\zeta - \zeta_1}{\sigma}|m\right) \\ &\text{or} \\ \eta(x,t) &= \eta_2 + (\eta_1 - \eta_2)\,\mathrm{cn}^2\left(\frac{\sqrt{3(\eta_1 - \eta_3)}}{2}(x - ct - x_0)|m\right)\end{aligned} \tag{4.14}$$

This is the periodic, or cnoidal, solution of the KdV equation, where the constants f_1 and f_2 denotes peak and trough elevation, respectively, and f_3 is a parameter that only affects the shape of the wave. Any cnoidal wave is completely determined as long as these three constants are fixed.

Note: when applying equation (4.8) the $\pm$ in equation (4.12) becomes redundant. The constant ζ_1 denotes the phase shift and can easily be ignored.

Since $0 \leq \mathrm{cn}^2 \leq 1$ the amplitude of this solution can be regarded as:

$$a_0 = \frac{1}{2}(f_1 - f_2) = \frac{1}{2}H$$

where $H = f_1 - f_2$ denotes the wave height.

By comparing equations (4.6) and (4.7) we get the phase speed:

$$c = 1 + \frac{1}{2}(f_1 + f_2 + f_3)$$

We can also obtain an expression for the wavelength, λ, by setting $\psi = \pi/2$ in equation (4.12), remembering that the distance from the trough to the crest equals one half wavelength:

$$\lambda = 2\int_{\zeta_1}^{\zeta_2} d\zeta = 2\sigma \int_0^{\pi/2} \frac{d\psi}{\sqrt{1 - m\sin^2\psi}} = 2\sigma K(m) \tag{4.15}$$

As with the solitary wave solution, the nonlinearity of the periodic solution is also apperent, due to the fact that propagation speed, wavelength and shape are all dependent on the amplitude.

Since the wave oscillates about the equilibrium level of the surface, the mean value of the surface displacement over one wavelength must be equal to zero. This statement can be expressed as the following:

$$0 = 2\int_{\zeta_1}^{\zeta_2} f(\zeta)d\zeta = 2\int_{\zeta_1}^{\zeta_2} f_2 + (f_1 - f_2)\,\mathrm{cn}^2\left(\frac{\zeta}{\sigma}|m\right) d\zeta \tag{4.16}$$

By using equation (4.11) and the second of equations (4.13) we can change

variables from ζ to ψ as follows:

$$\begin{aligned}
0 &= 2\int_0^{\pi/2} f_2 + (f_1 - f_2)\cos^2\psi \frac{d\zeta}{d\psi}\, d\psi \\
&= 2\sigma \int_0^{\pi/2} \frac{f_1 - (f_1 - f_2)\sin^2\psi}{\sqrt{1 - m\sin^2\psi}}\, d\psi \\
&= 2\sigma \int_0^{\pi/2} \frac{f_1 - m(f_1 - f_3)\sin^2\psi}{\sqrt{1 - m\sin^2\psi}}\, d\psi \\
&= 2\sigma \int_0^{\pi/2} \frac{f_1(1 - m\sin^2\psi) - f_3(1 - m\sin^2\psi) + f_3}{\sqrt{1 - m\sin^2\psi}}\, d\psi \\
&= 2\sigma(f_1 - f_3)\int_0^{\pi/2} \sqrt{1 - m\sin^2\psi}\, d\psi + 2\sigma f_3 \int_0^{\pi/2} \frac{1}{\sqrt{1 - m\sin^2\psi}}\, d\psi \\
&= 2\sigma\Big((f_1 - f_3)E(m) + f_3 K(m)\Big)
\end{aligned}$$

This is equivalent with:

$$0 = \frac{f_1 - f_2}{m}E(m) + f_3 K(m)$$

The constants, f_1, f_2 and f_3, can now be expressed in terms of wave height, H, and the elliptic parameter, m:

$$\begin{aligned}
f_1 &= \frac{H}{m}\left(1 - \frac{E(m)}{K(m)}\right), \\
f_2 &= \frac{H}{m}\left(1 - m - \frac{E(m)}{K(m)}\right) \\
\text{and} \quad f_3 &= -\frac{H}{m}\frac{E(m)}{K(m)}
\end{aligned} \tag{4.17}$$

Thus, fixing H and m is enough to specify any cnoidal wave, as long as the undisturbed water level is set to zero.

The figure below shows the cnoidal wave in one instant in time for $H = 0.1$ and $m = 0.5$:

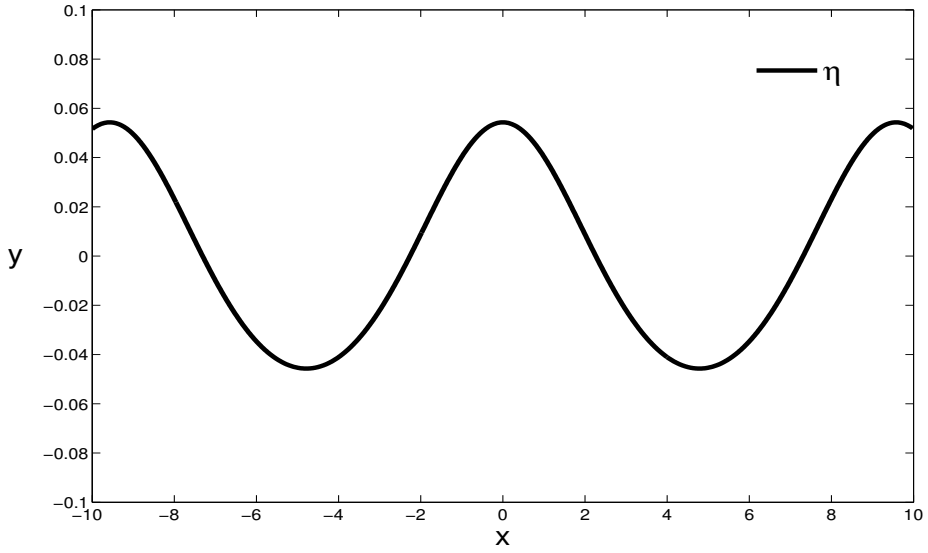

Figure 4.3: Cnoidal wave

As mentioned before, there is a close relationship between the cnoidal and solitary wave solutions of the KdV equation, namely that the solitary wave may be described as a limiting case of the cnoidal wave. The cnoidal solution is of course periodic with a finite wavelength, and the solitary wave is not. However, the solitary wave may also be though of as being periodic, but with an infinite wavelength. Thus, we should obtain the solitary wave by letting the wavelength of the cnoidal solution tend to infinity.

The solitary wave requires two simple zeros of the cubic F to coalesce to form a double zero. We accomplish this by letting $f_3 \to f_2^-$, with f_1 fixed. In this limit we get $m \to 1^-$, and a property of the elliptic function cn, is that $\mathrm{cn}(u|m) \to \mathrm{sech}(u)$ as $m \to 1^-$. By doing this, we can replace cn^2 by sech^2 in equation (4.14) to obtain:

$$f(\zeta) = f_2 + (f_1 - f_2)\,\mathrm{sech}^2(\zeta/\sigma) \tag{4.18}$$

Where the corresponding limiting values of c and σ are:

$$c = 1 + f_2 + \frac{1}{2}f_1 \quad \text{and} \quad \frac{1}{\sigma^2} = \frac{3(f_1 - f_2)}{4}$$

If we now choose $f_2 = 0$, which only readjusts the undisturbed water level below the solitary wave, we can denote the wave height by $f_1 = H$, and thus we have obtained the solitary wave, equation (4.4):

$$f(x - ct) = \eta(x, t) = H \operatorname{sech}^2 \left(\frac{\sqrt{3H}}{2}(x - ct) \right) \tag{4.19}$$

With $c = 1 + \frac{H}{2}$.

In the limit $m \to 1^-$ it is easy to see that the complete elliptic integral of the first kind, $K(m)$ tends to infinity, which also implies that the wavelength tends to infinity, as it should.

In the other limiting case, where $m \to 0^+$, the cnoidal wave becomes a linear wave, corresponding to the linearized version of the KdV equation. This is easy to see if we write the parameter m in terms of the amplitude, $a_0 = (f_1 - f_2)/2$:

$$m = \frac{2a_0}{f_1 - f_3}$$

From here it is clear that if m is to approach zero, then the amplitude must also approach zero, which is what characterizes a linear wave.

As a side note, it can be mentioned that the solutions of the KdV equation derived in this section does not exhaust the possibilities, but the remaining ones are not traveling waves and therefore has no relevance in this report.

Chapter 5

Breaking criterion and maximum wave height

5.1 Breaking criterion

In this section we formulate a breaking criterion for surface gravity waves in the Boussinesq parameter regime. We determine the onset of breaking at the point where the propagation speed (i.e. phase speed) of the traveling wave catches up with the horizontal particle speed of the fluid, evaluated at the surface. For both the solitary and periodic solutions of the KdV equation we have that wave height and propagation speed are dependent, hence the breaking criterion can be used to determine a maximum height, $H_{\max}$, for these waves.

As mentioned earlier, when deriving the KdV equation there also appears an expression for the horizontal component of the velocity field of the flow. This can be formulated in terms of the surface displacement, η, and its spatial derivatives. Thus we can apply the breaking criterion to both the solitary and periodic solutions, since expressions for the propagation speeds are available. We start with the solitary wave, and then go on to do the same with the periodic.

The breaking criterion is formulated as follows:

$$\phi_x(x, 1+\eta, t) \geq c \tag{5.1}$$

This is similar to the one found in [3].

Beyond this point the approximation, and thus the KdV equation itself is no longer valid as a physical model. In fact, the approximation ceases

to be valid before breaking (by this definition) occurs, since when the wave profile becomes sufficiently steep, α and β are no longer of the same order of magnitude. However, we neglect this here and assume the approximation is valid up to the breaking point.

From equation (3.41) we have that the horizontal component of the velocity field, approximated to second order in a series expansion, is given by:

$$u = \phi_x = w - \beta \frac{Y^2}{2} w_{xx}$$

We also have from (3.46) an expression for w of the same order in α and β:

$$w = \eta - \frac{1}{4}\alpha\eta^2 + \frac{1}{3}\beta\eta_{xx}$$

By combining these two, and again neglecting terms of $O(\alpha\beta, \beta^2)$, we obtain an expression for the horizontal component of the velocity field in terms of η and Y:

$$u = \phi_x = \eta - \frac{1}{4}\alpha\eta^2 + \beta\left(\frac{1}{3} - \frac{Y^2}{2}\right)\eta_{xx}$$

Since we now have ϕ_x to the correct order, we revert back to the original variables, again with $g = 1$ and $h_0 = 1$, and get the following expression for the horizontal velocity:

$$\phi_x = \eta - \frac{1}{4}\eta^2 + \left(\frac{1}{3} - \frac{Y^2}{2}\right)\eta_{xx} \tag{5.2}$$

The breaking criterion (5.1), can now be written as:

$$\eta - \frac{1}{4}\eta^2 + \left(\frac{1}{3} - \frac{(1+\eta)^2}{2}\right)\eta_{xx} \geq c \tag{5.3}$$

It is worth noting that there are also other ways of determining a breaking criterion for surface gravity waves, for instance using the vertical acceleration of the fluid particles.

5.2 Maximum height for the solitary wave

The solitary wave solution of the KdV equation is given by (4.4):

$$\eta = H \operatorname{sech}^2 \left(\frac{\sqrt{3H}}{2}(x - ct) \right)$$

and by twice differentiating this with respect to x we obtain:

$$\eta_{xx} = 3H^2 \operatorname{sech}^2 \left(\frac{\sqrt{3H}}{2}(x - ct) \right) \tanh^2 \left(\frac{\sqrt{3H}}{2}(x - ct) \right) - \frac{3}{2} H^2 \operatorname{sech}^4 \left(\frac{\sqrt{3H}}{2}(x - ct) \right)$$

Since the solitary wave retains its shape for all time we may evaluate at $(x, t) = (0, 0)$ for convenience, in which case we get:

$$\eta(0,0) = H$$
$$\eta_{xx}(0,0) = -\frac{3}{2}H^2$$

Substituting this into equation (5.2), and evaluating at the surface, gives the breaking criterion (5.1) as:

$$H - \frac{1}{4}H^2 - \frac{3}{2}\left(\frac{1}{3} - \frac{(1+H)^2}{2} \right) H^2 \geq \frac{1}{2}H + 1 \tag{5.4}$$

Setting the left hand side equal to the right hand side and rearranging terms yields:

$$P(H) = \frac{3}{4}H^4 + \frac{3}{2}H^3 + \frac{1}{2}H - 1 = 0 \tag{5.5}$$

The figure below shows a plot of $P(H)$.

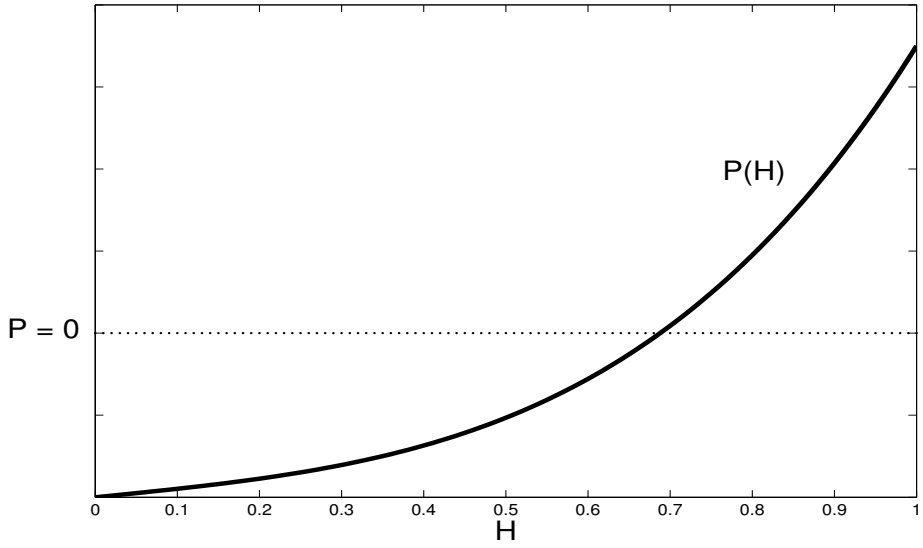

Figure 5.1: Maximum wave height polynomial for solitary wave

We see that P is a fourth order polynomial in H, and since $P'(H) = 3H^3 + \frac{9}{2}H^2 + \frac{1}{2} > 0$ for $H \geq 0$ and $P(0) < 0$ while $P(1) > 0$, it can have only one positive root which lies in $[0, 1]$.

This can be found numerically, using the bisection method, to obtain the following value of the maximum allowable wave heigh for the solitary wave:

$$H_{\text{max solitary}} = 0.6878525 \tag{5.6}$$

Where the error is less than 10^{-7}.

5.3 Maximum height for the periodic wave

The periodic wave solution of the KdV equation is given by (4.14):

$$f(\zeta) = f_2 + (f_1 - f_2)\,\mathrm{cn}^2\left(\frac{\zeta}{\sigma}|m\right)$$

By twice differentiating this with respect to x we obtain:

$$\begin{aligned} f_{xx} =& \frac{3}{2}(f_1 - f_2)(f_1 - f_3)\Bigg(\mathrm{sn}^2\left(\frac{\zeta}{\sigma}|m\right)\mathrm{dn}^2\left(\frac{\zeta}{\sigma}|m\right) + \\ & m^2\,\mathrm{sn}^2\left(\frac{\zeta}{\sigma}|m\right)\mathrm{cn}^2\left(\frac{\zeta}{\sigma}|m\right) - \mathrm{cn}^2\left(\frac{\zeta}{\sigma}|m\right)\mathrm{dn}^2\left(\frac{\zeta}{\sigma}|m\right)\Bigg) \end{aligned}$$

Evaluating at $\zeta = 0$ yields:

$$f(0) = f_1$$
$$f_{xx}(0) = -\frac{3}{2}(f_1 - f_2)(f_1 - f_3)$$

Substituting this into equation (5.2) gives the breaking criterion, (5.1), as:

$$f_1 - \frac{1}{4}f_1^2 - \frac{3}{2}\left(\frac{1}{3} - \frac{(1+f_1)^2}{2}\right)(f_1 - f_2)(f_1 - f_3) \geq 1 + \frac{1}{2}(f_1 + f_2 + f_3) \quad (5.7)$$

We continue by defining the following:

$$a = \frac{1}{m}\left(1 - \frac{E(m)}{K(m)}\right), \; b = \frac{1}{m}\left(1 - m - \frac{E(m)}{K(m)}\right) \quad \text{and} \quad c = \frac{1}{m}\frac{E(m)}{K(m)}$$

Such that we can write equations (4.17) as:

$$f_1 = Ha, \; f_2 = Hb \quad \text{and} \quad f_3 = -Hc$$

Substituting this into equation (5.7) and setting the left and right hand side equal gives:

$$\begin{aligned} Q_m(H) = &\frac{3}{4}H^4(a^4 + a^3c - a^3b - a^2bc) \\ &+ \frac{3}{2}H^3(a^2c + a^3 - a^2b - abc) \\ &+ \frac{1}{4}H^2(ac - bc - ab) \\ &+ \frac{1}{2}H(a - b + c) - 1 = 0 \end{aligned} \quad (5.8)$$

This is a fourth order polynomial in H, and by fixing a value for m it can be solved numerically to obtain the maximum allowable wave height for the cnoidal wave, $H_{\text{max cnoidal}}$. Since the periodic wave reduces to the solitary wave in 'the most nonlinear limit' ($m \to 1$), we look for real roots of (5.8) in the interval $[0, 1]$.

The figure below shows a plot of equation (5.8) for two different values of m. The dotted line represents $m = 0.2$ and the whole line represents $m = 0.7$.

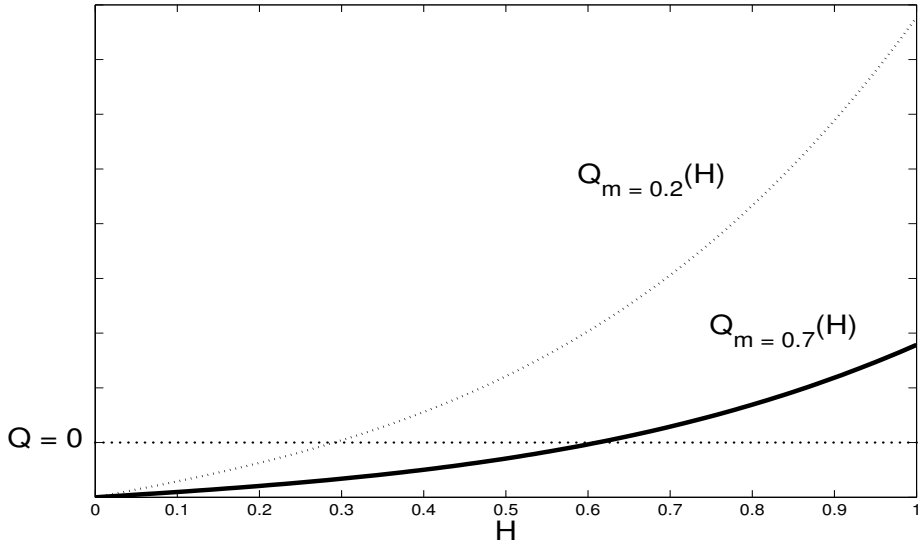

Figure 5.2: Maximum wave height polynomial for periodic wave

Different values of m and corresponding values of $H_{\text{max cnoidal}}$ are listed in the table below. The table also shows corresponding values of wave length, λ, the dimensionless parameters α and β, in addition to Stokes' number, $\mathcal{S}$, defined by the ratio α/β. All results were obtained using the bisection method, where the error is less than 10^{-7}:

m	$H_{\text{max cnoidal}}$	λ	α	β	$\mathcal{S}$
0.01	0.0196966	2.5912777	0.0098483	0.1489265	0.0661286
0.1	0.1698115	2.8575892	0.0849057	0.1224617	0.6933246
0.2	0.2908739	3.1781292	0.1454370	0.0990049	1.4689869
0.3	0.3820927	3.5071829	0.1910464	0.0812986	2.3499336
0.4	0.4548249	3.8496532	0.2274124	0.0674772	3.3702135
0.5	0.5151971	4.2181778	0.2575985	0.0562018	4.5834572
0.6	0.5666921	4.6327595	0.2833460	0.0465930	6.0813031
0.7	0.6113783	5.1284658	0.3056892	0.0380211	8.0399800
0.8	0.6504260	5.7811797	0.3252130	0.0299204	10.8692819
0.9	0.6840510	6.8292781	0.3420255	0.0214413	15.9517415

Table 5.1: This table shows the maximum wave height for the cnoidal solution of the KdV-equation, calculated for various values of the elliptic parameter, m. Corresponding values of wavelength, the dimensionless parameters α and β, in addition to Stokes' number, $\mathcal{S}$, are also listed.

The parameters α and β represents nonlinear and dispersive effects, respectively, and in this case they are given by $\alpha = \frac{1}{2}H_{\text{max cnoidal}}$ and $\beta = 1/\lambda^2$. A Stokes' number smaller than one therefore signifies a system where dispersive effects are dominant, while a Stokes' number greater than one signifies a system where nonlinear effects are dominant. From the table above it is clear that for small values of m dispersive effects dominate, while for values of m close to one, nonlinear effects dominate. This makes sense since we know that $m \to 0^+$ is the linear limit, while $m \to 1^-$ is the solitary wave limit.

It is also interesting that the maximum wave height seems to approach zero as m approaches zero. This becomes more evident if we plot maximum wave height as a function of m, using a finer resolution in m than displayed in the table above:

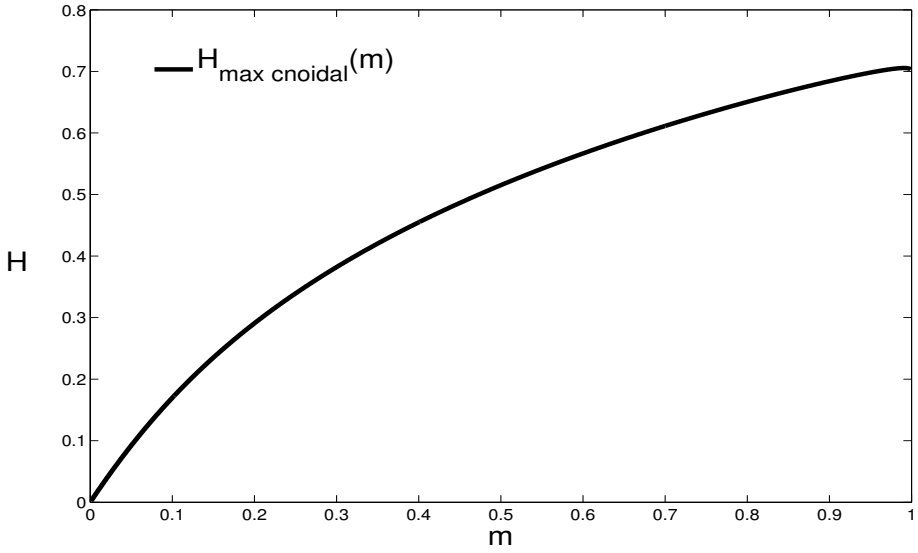

Figure 5.3: Maximum allowable wave height for the cnoidal solution as a function of m, plotted using 1000 values of $m \in (0, 1)$.

The maximum height for linear waves is of course not zero, this is simply a consequence of going 'outside' of the domain of validity of the Boussinesq approximation, where we assumed α and β are of the same order of magnitude. This also implies that the solitary wave technically is outside of this domain, since it has an infinite wavelength.

It is also worth noting that the limiting values of a, b and c as $m \to 1$ are:

$$a = 1, \ b = 0, \quad \text{and} \quad c = 0$$

Applying this to equation (5.8) gives the breaking criterion for the solitary wave, equation (5.5). This is also easy to see if we plot the maximum wave height of the cnoidal wave as a function of corresponding wave length:

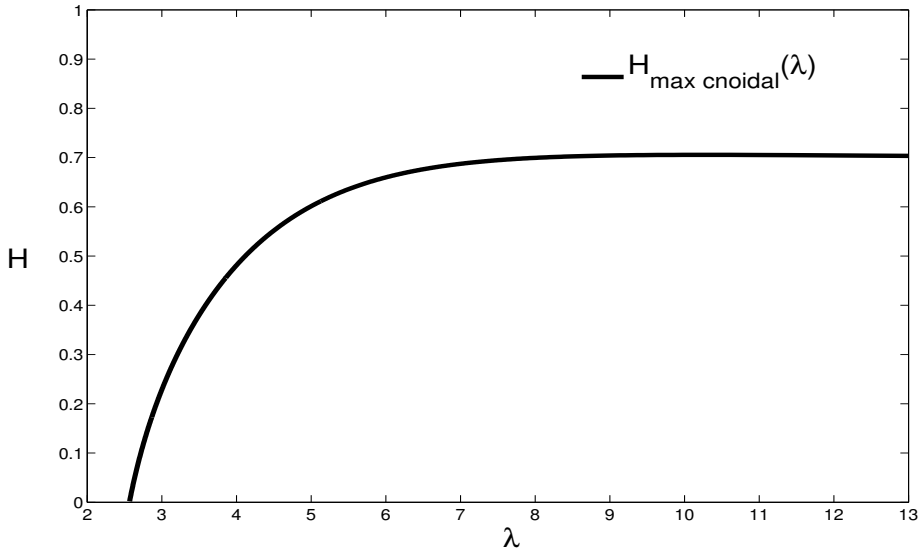

Figure 5.4: Maximum allowable wave height for the cnoidal solution as a function of wave length, plotted using the same resolution as in the figure above.

Chapter 6

The numerical methods

The KdV equation is a nonlinear partial differential equation of third order in spatial derivatives. Thus three boundary conditions are needed in addition to initial data. Finding stable numerical solutions to such initial boundary value problems can be quite difficult, especially close to the boundaries. In addition, the dispersive wave properties of the problem at hand require a high degree of resolution in the numerical computation to avoid the errors growing too large.

In this chapter two different numerical schemes for the KdV equation will be explained, where the first one is the so called 'summation by parts - simultaneous approximation term' (SBP-SAT) method, and the second one is an implicit finite difference (IFD) method. The SBP-SAT method can be shown to be numerically stable, but the computations are costly, yielding very long computation times. The implicit finite difference scheme is faster computational wise, but does not have the same stability properties as the SBP-SAT method.

6.1 Formulation of the problem

The goal is to use the KdV equation to simulate the evolution of an undular bore. We do this by setting a bore front as initial data, and then advance in time by integrating the KdV equation numerically.

The initial position of the bore front will be set to the origin, and the bore will then travel downstream in the positive x-direction. As before, we set the undisturbed water level at $h_0 = 1$, but we can still vary the strength of the bore, indicated by $\alpha = H_0/h_0$, by varying the initial wave height, H_0.

The initial data is given by:

$$\eta_0(x) = \frac{1}{2}H_0(1 - \tanh(kx)) \tag{6.1}$$

Where k is a model parameter denoting the steepness of the initial bore slope.

The figure below shows the initial profile with $\alpha = 0.4$ and $k = 1$.

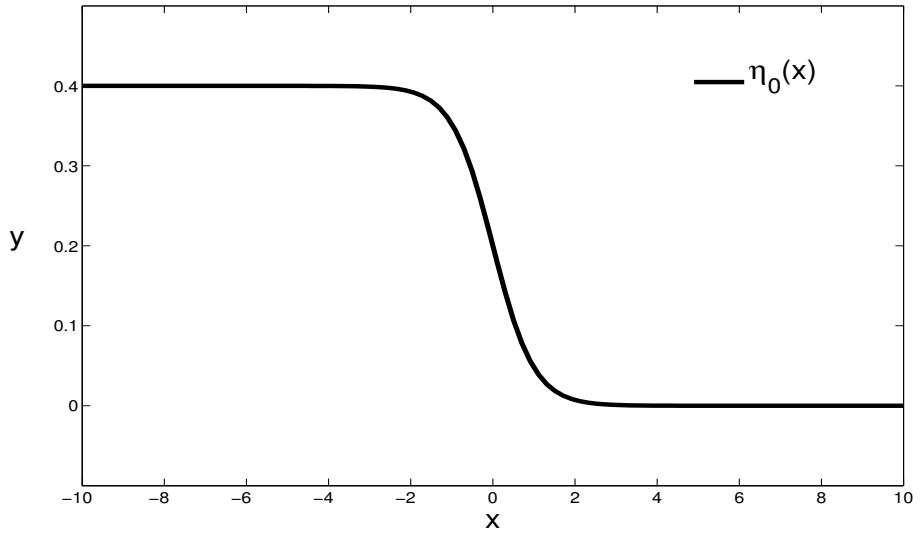

Figure 6.1: Initial profile

In the far field downstream of the bore front the surface elevation approaches zero, while in far field upstream it approaches H_0. These far field conditions are chosen to be the boundary conditions, which matches the initial data up to machine precision as long as the spatial domain is large enough. Thus care has to be taken to ensure this is the case. For the third boundary condition a homogenous Neumann condition is chosen on the right.

To summarize, the problem to be solved is given by:

$$\begin{aligned} \eta_t + \eta_x + \frac{3}{4}(\eta^2)_x + \frac{1}{6}\eta_{xxx} = 0,\ x \in [-l, l],\ t \geq 0 \\ \eta(x,0) = \eta_0(x), \\ \eta(-l,t) = H_0, \\ \eta(l,t) = 0, \\ \eta_x(l,t) = 0. \end{aligned} \tag{6.2}$$

We continue by discretizing the spatial domain, $[-l, l]$, uniformly using a finite set of points, $\{x_j\}_{j=0}^{N} \subset [-l, l]$, where $x_0 = -l$ and $x_N = l$, and $\delta x = 2l/N$ is the distance between two neighboring grid points. The time domain is also discretized uniformly using $t_n = n\delta t$, where $t_0 = 0$.

6.2 The energy method

The energy method makes it possible to predict the growth of the solution when the type of boundary conditions are specified. In this case we use Dirichlet-Neumann conditions, since these are the ones found in (6.2). The energy method can also be used to determine what type of boundary conditions will lead to a well-posed problem (assuming a unique solution exists).

In this section we apply the energy method on both the linear and non-linear continuous problems to show that Dirichlet-Neumann boundary conditions will lead to a well-posed problem.

If we denote the boundary and initial data by:

$$\begin{aligned} \eta(x,0) = f(x) \\ \eta(-l,t) = g_0(t) \\ \eta(l,t) = g_1(t) \\ \eta_x(l,t) = g_2(t) \end{aligned} \tag{6.3}$$

The condition for well-posedness is:

$$\frac{d}{dt}||\eta||^2 \leq 0 \tag{6.4}$$

When $||\cdot||$ denotes the L^2-norm, and $g_0 = g_1 = g_2 = 0$.

The 'energy' of the system is defined as $||\eta||^2$, so this condition simply states that there must be a non-growing 'energy' when no forcing is applied to the system. Although the term 'energy' is used, it need not be linked to some physical definition of energy for this approach to be valid.

We begin with the nonlinear problem, given by:

$$\eta_t + \eta_x + \frac{3}{2}\eta\eta_x + \frac{1}{6}\eta_{xxx} = 0,\ x \in [-l, l],\ t \geq 0 \tag{6.5}$$

with boundary and initial data specified by (6.3).

Multiplying with η and integrating over the spatial domain yields:

$$\frac{1}{2}\int_{-l}^{l}(\eta^2)_t dx + \frac{1}{2}\int_{-l}^{l}(\eta^2)_x dx + \frac{1}{2}\int_{-l}^{l}(\eta^3)_x dx + \frac{1}{6}\int_{-l}^{l}\eta\eta_{xxx} dx = 0 \tag{6.6}$$

Applying integration by parts on the last integral and rearranging terms yields:

$$\frac{d}{dt}||\eta||^2 = -\eta^2\Big|_{-l}^{l} - \eta^3\Big|_{-l}^{l} - \frac{1}{3}\eta\eta_{xx}\Big|_{-l}^{l} + \frac{1}{6}(\eta_x)^2\Big|_{-l}^{l} \tag{6.7}$$

Where we have also used the fact that: $\int_{-l}^{l}(\eta^2)_t dx = \frac{d}{dt}\int_{-l}^{l}\eta^2 dx = \frac{d}{dt}||\eta||^2$.

We continue by rewriting as follows:

$$\begin{aligned}\frac{d}{dt}||\eta||^2 =& -\eta\left(\eta + \eta^2 + \frac{1}{3}\eta_{xx}\right)\Big|_{x=l} - \eta\left(\eta + \eta^2 + \frac{1}{3}\eta_{xx}\right)\Big|_{x=-l} \\ &+ \frac{1}{6}(\eta_x)^2\Big|_{x=l} - \frac{1}{6}(\eta_x)^2\Big|_{x=-l} \\ =& -\frac{1}{6}(\eta_x)^2\Big|_{x=-l} \leq 0\end{aligned} \tag{6.8}$$

Thus, the problem (6.2) is well posed.

Going through the same analysis for the linear problem:

$$\eta_t + a\eta_x + b\eta_{xxx} = 0,\ x \in [-l, l],\ t \geq 0\ a, b > 0 \tag{6.9}$$

With boundary and initial data specified by (6.3), yields:

$$\begin{aligned}\frac{d}{dt}||\eta||^2 &= \eta(a\eta + 2b\eta_{xx})\Big|_{x=-l} - \eta(a\eta + 2b\eta_{xx})\Big|_{x=l} + b\eta_x^2\Big|_{x=l} - b\eta_x^2\Big|_{x=-l} \\ &= -b\eta_x^2\Big|_{x=-l} \leq 0\end{aligned} \tag{6.10}$$

Since the nonlinear problem is well posed, it is not necessary to show the same for the linear problem as well, but we will be needing equation (6.10) in the next section.

6.3 The SBP-SAT method

The idea of the SBP-SAT method is to augment finite difference-'summation by parts' (SBP) schemes with the SAT-technique to impose the boundary conditions weakly. This is done by adding penalty terms at each time step to enforce the boundaries towards the boundary data.

The first step is to define the SBP-operators which are designed to mimic the continuous energy estimate done in the previous section, but in a semi-discrete setting (time is left continuous). The SAT-terms can then be derived, and by adding these we impose the boundary conditions weakly and thus keep the energy of the system from growing. By doing this, we prove stability for the linear semi-discrete problem. This implies stability with respect to small perturbations also for the nonlinear semi-discrete problem, as long as the nonlinear problem is well-posed, and in addition has a bounded and smooth solution [19]. The next step is then to fit the SAT-terms to the semi-discrete nonlinear problem, and finally, discretize in time using a method that captures the eigenvalues of the semi-discrete problem, such as an explicit Runge-Kutta method. The size of the time step is then determined by the CFL-condition.

We start by defining the approximate function value at grid point x_j to be $u_j(t) \approx \eta(x_j, t)$, and denote the approximate solution vector by: $u = (u_0, u_1, \cdots, u_N)^T$.

The first derivative in the interior of the domain at grid point x_j is ap-

proximated by the following second order central difference formula:

$$\eta_x(x_j,t) \approx \frac{u_{j+1}-u_{j-1}}{2\delta x}\ , \qquad 1 \leq j \leq N-1$$

And at the endpoints we use the following first order forwards and backwards differences, respectively:

$$\eta(x_0,t) \approx \frac{u_1-u_0}{\delta x} \quad \text{and} \quad \eta(x_N,t) \approx \frac{u_N-u_{N-1}}{\delta x}$$

We can now define the SBP-operators, and we begin with the difference operator matrix, D:

$$D = \tfrac{1}{2\delta x}\begin{pmatrix} -2 & 2 & 0 & & \cdots & 0 \\ -1 & 0 & 1 & 0 & & \vdots \\ 0 & -1 & 0 & 1 & & \\ \vdots & & & \ddots & & \\ & & & -1 & 0 & 1 \\ 0 & \cdots & & & -2 & 2 \end{pmatrix}$$

Where $D = P^{-1}Q$. The matrices P and Q are given below:

$$P = \delta x \begin{pmatrix} \frac{1}{2} & 0 & \cdots & & 0 \\ 0 & 1 & 0 & & \vdots \\ \vdots & & \ddots & & \\ & & 0 & 1 & 0 \\ 0 & \cdots & & 0 & \frac{1}{2} \end{pmatrix}$$

$$Q = \tfrac{1}{2}\begin{pmatrix} -1 & 1 & 0 & \cdots & 0 \\ -1 & 0 & 1 & & \vdots \\ & & \ddots & & \\ & & -1 & 0 & 1 \\ 0 & \cdots & 0 & -1 & 1 \end{pmatrix}$$

The matrix P is symmetric positive definite, and $P = P^T$, such that P defines a discrete L^2-equivalent norm as: $||u||_P^2 = u^T P u$.

In addition we define the matrix B:

$$Q + Q^T = B = \begin{pmatrix} -1 & 0 & \cdots & & 0 \\ & 0 & & & \vdots \\ & & \ddots & & \\ & & & 0 & \\ 0 & \cdots & & 0 & 1 \end{pmatrix}$$

And the unit vectors: $\hat{e_0} = (1, 0, \cdots, 0)^T$ and $\hat{e_N} = (0, \cdots, 0, 1)^T$.

Applying this to equation (6.9) gives:

$$u_t + aDu + bDDDu = 0$$

If we set $a = 1 + \frac{3}{2}u$ and $b = \frac{1}{6}$, we have the original nonlinear equation, but for now we think of a as being 'frozen' in space and time, and thus may be treated as a constant in the following analysis.

We continue by multilying from the left by $u^T P$ to obtain:

$$u^T P u_t + a u^T P P^{-1} Q u + b u^T P P^{-1} Q D D u = 0$$

And rewrite the last term on the left as follows:

$$b u^T Q D D u = b u^T B D D u - b u^T Q^T D D u = b u^T B D D u - b (Du)^T Q D u$$

Thus we have:

$$u^T P u_t + a u^T P P^{-1} Q u + b u^T B D D u - b (Du)^T Q D u = 0$$

Adding the transpose of the equation gives:

$$\frac{d}{dt} ||u||_P^2 = -a u^T B u - 2 b u^T B D D u + b (Du)^T B D u$$

Since $u^T P u_t + u_t^T P u = \frac{d}{dt}(u^T P u)$.

Which can also be written as:

$$\begin{aligned} \frac{d}{dt} ||u||_P^2 &= a u_0^2 - a u_N^2 + 2 b u_0 (DDu)_0 - 2 b u_N (DDu)_N + (Du)_N^2 - (Du)_0^2 \\ &= u_0 (a u_0 + 2 b (DDu)_0) - u_N (a u_N + 2 b (DDu)_N) \\ &\quad + b (Du)_N^2 - b (Du)_0^2 \end{aligned} \tag{6.11}$$

This is the discrete equivalent of equation (6.10), and thus the next step is to derive the penalty terms to ensure a non growing energy, which in turn implies stability for the semi-discrete problem. The SBP-SAT discretization of the problem (6.9) is given by:

$$u_t + aDu + bDDDu = P^{-1}SAT \tag{6.12}$$

Multiplying from the left by $u^T P$ and adding the transpose yields:

$$\begin{aligned}\frac{d}{dt}||u||_P^2 = u_0(au_0 + 2b(DDu)_0) - u_N(au_N + 2b(DDu)_N) \\ + b(Du)_N^2 - b(Du)_0^2 + 2u^T SAT\end{aligned} \tag{6.13}$$

The semi-discrete problem is now stable if we choose:

$$\begin{aligned}SAT = &-\frac{1}{2}(a + 2b(DD)^T)\hat{e_0}(u_0 - g_0) + \frac{1}{2}(a + 2b(DD)^T)\hat{e_N}(u_N - g_1) \\ &- \frac{1}{2}bD^T\hat{e_N}((Du)_N - g_2)\end{aligned} \tag{6.14}$$

This can be seen by substituting back into equation (6.13):

$$\begin{aligned}\frac{d}{dt}||u||_P^2 = &-b(Du)_0^2 + g_0(au_0 + 2b(DDu)_0) - g_1(au_N + 2b(DDu)_N) + bg_2(Du)_N \\ \implies &\frac{d}{dt}||u||^2 = -b(Du)_0^2 \leq 0 \quad \text{when} \quad g_0 = g_1 = g_2 = 0\end{aligned}$$

Now it only remains to derive the SAT-terms for the nonlinear problem. That means we must set:

$$a = 1 + \frac{3}{2}u \quad \text{and} \quad b = \frac{1}{6}$$

But we can not just insert this into equation (6.14), we also must pay attention to the direction of u at the boundaries. From equation (6.13) we see that for the left boundary only positive values of u leads to a growing

energy, while on the right boundary negative values of u leads to a growing energy. Thus, we must define:

$$a^+ = 1 + \frac{3}{2}\max(u_0, 0) \text{ on the left boundary}$$
$$a^- = 1 + \frac{3}{2}\min(u_N, 0) \text{ on the right boundary}$$

Inserting this to equation (6.14) yields:

$$\begin{aligned} SAT = &-\frac{1}{2}(a^+ + \frac{1}{3}(DD)^T)\hat{e_0}(u_0 - g_0) \\ &+\frac{1}{2}(a^- + \frac{1}{3}(DD)^T)\hat{e_N}(u_N - g_1) \\ &-\frac{1}{12}D^T\hat{e_N}((Du)_N - g_2) \end{aligned} \tag{6.15}$$

We may now discretize in time, using $u_j^n \approx \eta(x_j, t_n)$ such that $u^n = (u_0^n, u_1^n, \cdots, u_N^n)$, to set up the following difference equation for the nonlinear problem, (6.2):

$$\frac{u^{n+1} - u^n}{\delta t} = -Du^n - \frac{3}{4}D(u^n)^2 - \frac{1}{6}DDDu^n + P^{-1}SAT = F(u^n) \tag{6.16}$$

and use an explicit 'Runge-Kutta 4'-method to advance in time:

$$\begin{aligned} u^{n+1} &= u^n + \frac{\delta t}{6}(k_1 + 2k_2 + 2k_3 + k_4) \\ \text{where } k_1 &= F(u^n), \\ k_2 &= F\left(u^n + \frac{\delta t}{2}k_1\right), \\ k_3 &= F\left(u^n + \frac{\delta t}{2}k_2\right), \\ \text{and } k_4 &= F(u^n + \delta t k_3) \end{aligned} \tag{6.17}$$

The size of the time step is governed by the CFL-condition, which states that $\delta t \sim \delta x^n$ where n is determined by the order of the highest derivative, which in this case is $n = 3$.

6.4 The implicit finite difference method

In this section the implicit finite difference method to solve the KdV equation is explained. The scheme presented here is largely the same as the one found

in [5], only with small modifications.

As in the previous section, finite difference stencils are used to approximate the spatial derivatives, while to advance in time, an explicit Adams-Bashforth method is used on the nonlinear terms while an implicit Crank-Nicolson method is used on the linear terms. Both methods are of second order, and while this does not automatically yield a second order scheme for the full equation, numerical experiments in [5] suggest that this is in fact the case.

Given a problem, $y' = f(t, y)$, the explicit Adams-Bashforth and implicit Crank-Nicolson methods are given respectively by:

$$\begin{aligned}\frac{y_{n+1} - y_n}{h} &= \frac{3}{2}f(t_n, y_n) - \frac{1}{2}f(t_{n-1}, y_{n-1}) \\ \frac{y_{n+1} - y_n}{h} &= \frac{1}{2}\bigg(f(t_{n+1}, y_{n+1}) + f(t_n, y_n)\bigg)\end{aligned}$$

where $t_n = nh$ and $y_n = y(t_n)$.

Now, instead of tackling the problem (6.2) directly, we define the function:

$$\xi(x, t) \equiv \eta(x, t) - \eta_0(x) \tag{6.18}$$

Such that upon substituting for $\eta(x, t)$ in (6.2) we have the problem in terms of ξ and η_0 which now has homogenous Dirichlet and Neumann boundary conditions. Doing this, the problem (6.2) becomes:

$$\begin{aligned}\xi_t + \xi_x + \frac{3}{4}(\xi^2)_x + \frac{3}{2}(\eta_0\xi)_x + \frac{1}{6}\xi_{xxx} = \ -F, \ x \in [-l, l], \ t \geq 0, \\ \xi(x, 0) = 0, \\ \xi(-l, t) = 0, \\ \xi(l, t) = 0, \\ \xi_x(l, t) = 0.\end{aligned} \tag{6.19}$$

Where $F \equiv \eta_0' + \frac{3}{2}\eta_0\eta_0' + \frac{1}{6}\eta_0'''$.

We continue with the same spatial and temporal discretization as in the previous sections, and define the approximate function value at grid point x_j and time t_n to be: $v_j^n \approx \xi(x_j, t_n)$.

The first and third spatial derivatives in the interior of the domain at grid point x_j are approximated using the following second order central difference formulas:

$$\xi_x(x_j,t) \approx \frac{v_{j+1}-v_{j-1}}{2\delta x}\ , \qquad 1 \le j \le N-1$$
$$\xi_{xxx}(x_j,t) \approx \frac{v_{j+2}-2v_{j+1}+2v_{j-1}-v_{j-2}}{2\delta x^3}\ , \qquad 2 \le j \le N-2$$

The third derivate formula gives two grid points on each side for which the scheme is not valid, while the first derivative formula gives one point on each side. However, from the Dirichlet conditions we have that $v_0 = 0$ and $v_N = 0$, so we need only solve the problem (6.19) at the grid points $\{x_j\}_{j=1}^{N-1}$. This leaves us with only two points for which the third derivative stencil is not valid.

From the Neumann condition we have that $\xi_x(l,t) = 0$, so by writing this as a central difference approximation we get that:

$$\frac{v_{N+1}-v_{N-1}}{2\delta x} = 0 \implies v_{N+1} = v_{N-1}$$

This enables us to use the third derivative approximation at grid point x_{N-1} as follows:

$$\xi_{xxx}(x_{N-1},t) \approx \frac{v_{N+1}-2v_N+2v_{N-2}-v_{N-3}}{2\delta x^3} = \frac{v_{N-1}+2v_{N-2}-v_{N-1}}{2\delta x^3}$$

As there is no Neumann condition on the left we use a forward difference formula to approximate the third derivative at grid point x_1:

$$\xi_{xxx}(x_1,t) \approx \frac{-v_4+6v_3-12v_2+10v_1-3v_0}{2\delta x^3} = \frac{-v_4+6v_3-12v_2+10v_1}{2\delta x^3}$$

Thus, we define the approximate solution vector as: $v^n = (v_1^n, v_2^n, \cdots, v_{N-1}^n)^T$.

Now that we can approximate the first and third spatial derivative at all grid points, we can define the following $(N-1)\times(N-1)$ difference matrix operators for the first derivative:

$$D_1 = \frac{1}{2\delta x}\begin{pmatrix} 0 & 1 & 0 & & & \cdots & 0 \\ -1 & 0 & 1 & 0 & & & \vdots \\ 0 & -1 & 0 & 1 & 0 & & \\ \vdots & & & \ddots & & & \\ 0 & \cdots & & & & 0 & 1 \\ 0 & \cdots & & & & -1 & 0 \end{pmatrix}$$

And for the third derivative:

$$D_3 = \frac{1}{2\delta x^3}\begin{pmatrix} 10 & -12 & 6 & -1 & 0 & \cdots & 0 \\ 2 & 0 & -2 & 1 & 0 & \cdots & 0 \\ -1 & 2 & 0 & -2 & 1 & 0 & \\ 0 & -1 & 2 & & \ddots & & \\ \vdots & & & \ddots & & \ddots & 1 \\ & & & & \ddots & 0 & -2 \\ 0 & & \cdots & & -1 & 2 & 1 \end{pmatrix}$$

We may now set up the following difference equation:

$$\frac{v^{n+1} - v^n}{\delta t} = -\frac{3}{4}D_1(v^n)^2 - \frac{3}{2}D_1 v^n \tilde{\eta_0} - \frac{1}{6}D_3 v^n - D_1 v^n - \tilde{F} \tag{6.20}$$

where $\tilde{\eta_0}$ is the initial data projected onto the grid $\{x_j\}_{j=1}^{N-1}$, and $\tilde{F}$ is the right hand side of (6.2) also projected onto $\{x_j\}_{j=1}^{N-1}$, such that $\tilde{\eta_0} = (\eta_0(x_1), \eta_0(x_2), ..., \eta_0(x_{N-1}))^T$ and $\tilde{F} = (F(x_1), F(x_2), ..., F(x_{N-1}))^T$.

By applying the Adams-Bashford method on the two first terms on the right, and the Crank-Nicolson method on the next two terms we get:

$$\begin{aligned} \frac{v^{n+1} - v^n}{\delta t} = &-\frac{3}{4}D_1\left[\ 3\left(\frac{1}{2}(v^n)^2 + v^n\tilde{\eta_0}\right) - \left(\frac{1}{2}(v^{n-1})^2 + v^{n-1}\tilde{\eta_0}\right)\ \right] \\ &-\frac{1}{2}\left[\ D_1\left(v^{n+1} + v^n\right) + \frac{1}{6}D_3\left(v^{n+1} + v^n\right)\ \right] - \tilde{F} \end{aligned} \tag{6.21}$$

At each time step this equation has to be solved for v^{n+1} to advance in time. By defining the matrix $E = (I + \frac{\delta t}{2}D_1 + \frac{\delta t}{12}D_3)$ for convenience, we do

this as follows (I denotes the $(N-1)\times(N-1)$ identity matrix):

$$\begin{aligned} v^{n+1} = {} & E^{-1}\left(I - \frac{\delta t}{2}D_1 - \frac{\delta t}{12}D_3\right)v^n \\ & - \frac{3\delta t}{4}E^{-1}D_1\left[\ 3\left(\frac{1}{2}(v^n)^2 + v^n\tilde{\eta_0}\right) - \left(\frac{1}{2}(v^{n-1})^2 + v^{n-1}\tilde{\eta_0}\right)\ \right] \\ & - \delta t E^{-1}\tilde{F} \end{aligned} \tag{6.22}$$

This method requires function values at two previous time steps to calculate the next one, so at the very first iteration a different approach is needed. One way of fixing the problem is to use a forward Euler method on the nonlinear terms at the first time step. This method has a local truncation error of order two and any instability issues will not be a problem for one single time step. By doing this, we get the following difference equation for the first time step:

$$\frac{v^2 - v^1}{\delta t} = -\frac{3}{2}D_1\left[\frac{1}{2}(v^1)^2 + v^1\tilde{\eta_0}\right] - \frac{1}{2}\left[\ D_1(v^2+v^1) + \frac{1}{6}D_3(v^2+v^1)\ \right] - \tilde{F} \tag{6.23}$$

Which can be solved for v^2 in a similar manner as above.

At each time step the approximate solution to the problem (6.2) is then given by equation (6.18).

6.5 Stability analysis for the implicit finite difference method

In this section the stability of the scheme (6.21) is analyzed. This is done in the same way as in [5], where the linear and nonlinear parts are analyzed separately. The right hand side of equation (6.19) is ignored in this analysis as it will not affect stability in any way. Also note that boundary effects are not part of this analysis, although they may contribute in a significant way to the instability of the scheme, but with a large enough spatial domain we assume these can be neglected.

By defining:

$$v_j^n = \gamma^n e^{ij\delta x} \tag{6.24}$$

where γ is the growth factor, the stability criterion is that $|\gamma| \leq 1$ when inserting this into (6.21) and solving for γ. There might be some restrictions on the choices of δt and δx for this to be fulfilled, in which case there will be

a region of stability for γ in the complex plane.

We start with the linear part of (6.21), which at grid point x_j takes the form:

$$\begin{aligned}\frac{v_j^{n+1}-v_j^n}{\delta t} =& -\frac{1}{2}\left(\frac{v_{j+1}^{n+1}-v_{j-1}^{n+1}}{2\delta x}+\frac{v_{j+1}^{n}-v_{j-1}^{n}}{2\delta x}\right)\\ &-\frac{1}{12}\left(\frac{v_{j+2}^{n+1}-2v_{j+1}^{n+1}+2v_{j-1}^{n+1}-v_{j-2}^{n+1}}{2\delta x^3}+\frac{v_{j+2}^{n}-2v_{j+1}^{n}+2v_{j-1}^{n}-v_{j-2}^{n}}{2\delta x^3}\right)\end{aligned} \tag{6.25}$$

After inserting (6.24) and solving for γ we get:

$$\gamma = \frac{1 - i\frac{\delta t}{\delta x}\left(\frac{1}{2}\sin(\delta x) + \frac{1}{6\delta x^2}\sin(\delta x) - \frac{1}{12\delta x^2}\sin(2\delta x)\right)}{1 + i\frac{\delta t}{\delta x}\left(\frac{1}{2}\sin(\delta x) + \frac{1}{6\delta x^2}\sin(\delta x) - \frac{1}{12\delta x^2}\sin(2\delta x)\right)} \tag{6.26}$$

Since the numerator and denominator make up a complex conjugate pair we have $|\gamma| = 1$ no matter the choice of δt and δx. In other words, the linear part of the scheme (6.21) is unconditionally stable.

For the nonlinear part we assume that the solution is bounded by some constant $A > 0$, such that we can write equation (6.19) as:

$$\xi_t + 3A\xi_x = 0, \quad \text{when} \quad \xi \leq A \tag{6.27}$$

By writing this as a difference equation at grid point x_j and applying the Adams-Bashforth method we get:

$$\frac{v_j^{n+1}-v_j^n}{\delta t} = -3A\left(\frac{3}{2}\frac{v_{j+1}^{n}-v_{j-1}^{n}}{2\delta x} - \frac{1}{2}\frac{v_{j+1}^{n-1}-v_{j-1}^{n-1}}{2\delta x}\right) \tag{6.28}$$

By inserting equation (6.24) and rearranging terms we get the following quadratic equation in γ:

$$\gamma^2 + \gamma\left(i\frac{9}{2}\frac{A\delta t}{\delta x}\sin(\delta x) - 1\right) - i\frac{3}{2}\frac{A\delta t}{\delta x}\sin(\delta x) = 0 \tag{6.29}$$

This equation can be solved using the quadratic formula which yields two expressions for γ, depending on the sign of the square root. They will be denoted by γ_+ and γ_-, and the stability criterion is $\max(|\gamma_+|, |\gamma_-|) \leq 1$.

As the $\sin(\delta x)$-factor does not contribute to growth of γ we neglect this and in addition define $\sigma = \frac{A\delta t}{\delta x} > 0$ which gives the formula:

$$\gamma^2 + \gamma\left(i\frac{9}{2}\sigma - 1\right) - i\frac{3}{2}\sigma = 0 \tag{6.30}$$

which gives the following expressions for γ_+ and γ_-:

$$\begin{aligned}\gamma_+ &= \frac{1}{2} - i\frac{9}{4}\sigma + \frac{1}{2}\sqrt{1 - \frac{81}{4}\sigma^2 - i3\sigma} \\ \gamma_- &= \frac{1}{2} - i\frac{9}{4}\sigma - \frac{1}{2}\sqrt{1 - \frac{81}{4}\sigma^2 - i3\sigma}\end{aligned} \tag{6.31}$$

The figure below shows a plot of $|\gamma_+|$ and $|\gamma_-|$.

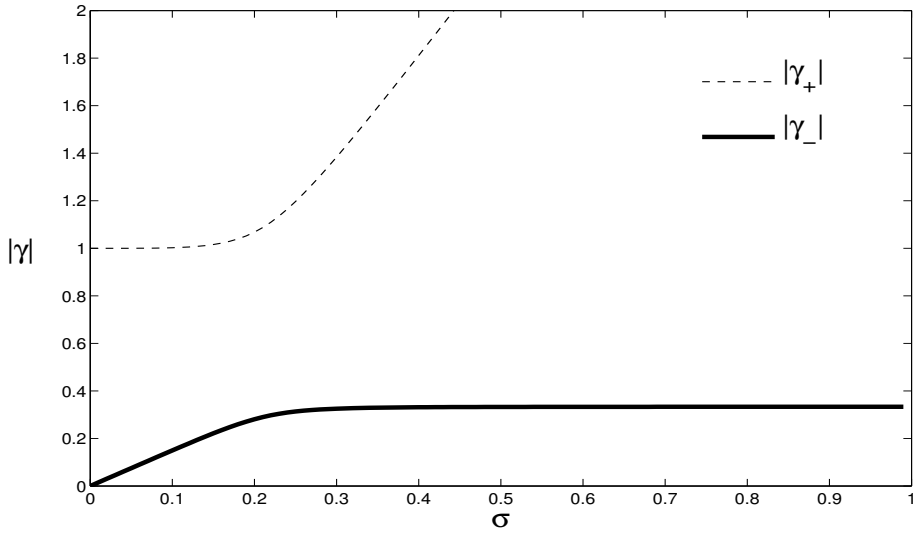

Figure 6.2: Growth factors

From the figure it is clear that $\max(|\gamma_+|, |\gamma_-|) = |\gamma_+|$, and although it is outside of the domain considered, we have that $|\gamma_+(0)| = 1$. Thus there is never stability for the nonlinear part of the scheme (6.21), but by choosing appropriate values for δt and δx we can make the growth factor as close to one as we would like. This is not an ideal situation, but as long as care is taken when choosing values for δx and δt, stability is achieved in practice.

6.6 Numerical calculation of particle and phase speed

In this section we show how the phase and horizontal particle speeds of the undular bore is calculated numerically. As in section 5.1 we can then find the maximum wave height of the bore at the point when the horizontal particle speed catches up with the phase speed.

In order to calculate the horizontal particle velocity we will need to approximate the second spatial derivative of the surface, and we do this by the following second order central difference formula:

$$\eta_{xx}(x_j, t_n) \approx \frac{u^n_{j-1} - 2u^n_j + u^n_{j+1}}{\delta x^2}$$

where $\eta(x_j, t_n) \approx u^n_j$.

We define the approximate horizontal velocity at grid point x_j and time t^n evaluated at the surface as $w^n_j \approx \phi_x(x_j, 1 + \eta(x_j, t_n), t_n)$, such that when we apply equation (5.2) we get:

$$w^n_j = u^n_j - \frac{1}{4}(u^n_j)^2 + \left(\frac{1}{3} + \frac{(1 + u^n_j)^2}{2}\right) \frac{u^n_{j-1} - 2u^n_j + u^n_{j+1}}{\delta x^2} \tag{6.32}$$

At each time step w^n_j is then calculated at the position of the bore front, or equivalently, at the position of maximum amplitude. As long as this point is in the interior of the domain, we need not worry about points where the second derivative stencil is not valid.

The phase speed can be found by measuring how any point on the wave profile moves in time. For convenience, we use the position of the bore front, and then calculate the phase speed at each time step by the same second order central difference method as above:

$$c^n = \frac{1}{\delta t}\left(s^{n-1} - 2s^n + s^{n+1}\right) \tag{6.33}$$

where c^n denotes the phase speed at time $t = t^n$, and s^n is the position of the bore front at time $t = t^n$.

To smooth out the curves, a moving average is then taken at each time step over a number of neighboring points.

Chapter 7

Results

This chapter is devoted to some numerical calculations, using both the IFD method and the SBP-SAT method. First off, we approximate the critical bore strength for which breaking first occurs. We then increase the bore strength by small increments and calculate the maximum wave heights. These values can then be compared with the maximum wave heights found for the solitary and periodic waves in sections 5.2 and 5.3.

All calculations were done using MatLab, with the following spatial and temporal resolution:

$$\delta x = 0.1 \quad \text{and} \quad \delta t = 0.001 \tag{7.1}$$

This should be good enough to ensure stability for the SBP-SAT method and (almost) stability for the IFD scheme. The MatLab source code can be found in the appendix.

7.1 Threshold for breaking

In this section we aim to find the threshold for which the bore transitions from purely undular to start exhibit breaking. This threshold is defined in terms of the ratio α, and as mentioned before, it is found experimentally to be $\alpha = 0.28$. We will therefore use this value of α as a starting point, and then proceed with small increments until the breaking criteria is reached, i.e. when the horizontal particle speed of the fluid exceeds the phase speed. A similar study was done in [3], where numerical studies of Boussinesq models for undular bores found that breaking appears for $\alpha > 0.379$. We expect to obtain a result not too far from this.

Since it requires a large amount of steps to reach the breaking point for small values of α, the results in this section were obtained using the implicit finite difference scheme, explained in section 6.4, because it runs much faster than the SBP-SAT method.

It should also be noted that a limit was set at $N_t = 120\ 000$ to keep the accumulated error from growing too large.

The figure below shows the phase speed and horizontal particle speed when $\alpha = 0.28$. Clearly there is no breaking in this case.

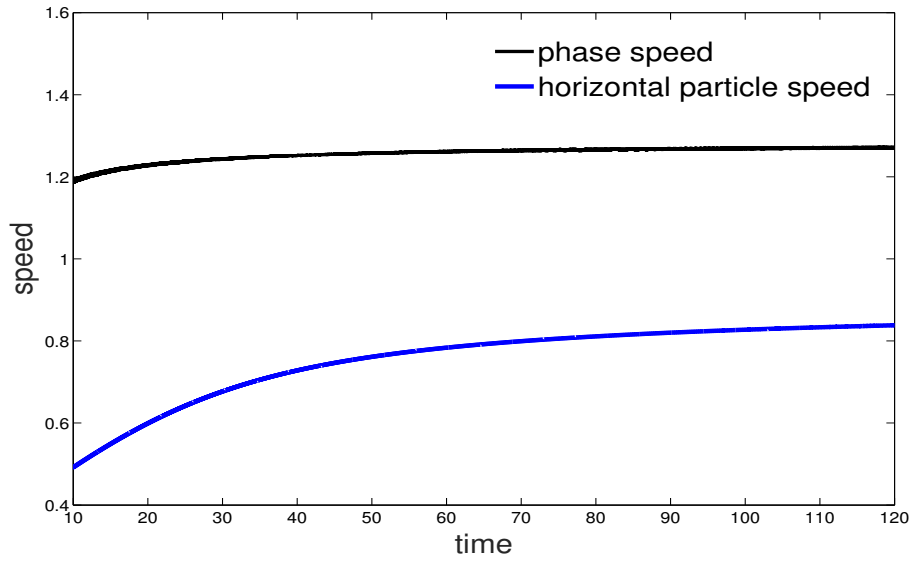

Figure 7.1: Phase speed and horizontal particle speed for $\alpha = 0.28$

After increasing α by increments of 0.001 breaking is obtained for $\alpha = 0.358$. We denote this ratio by: α_{crit}. This is shown in the figure below.

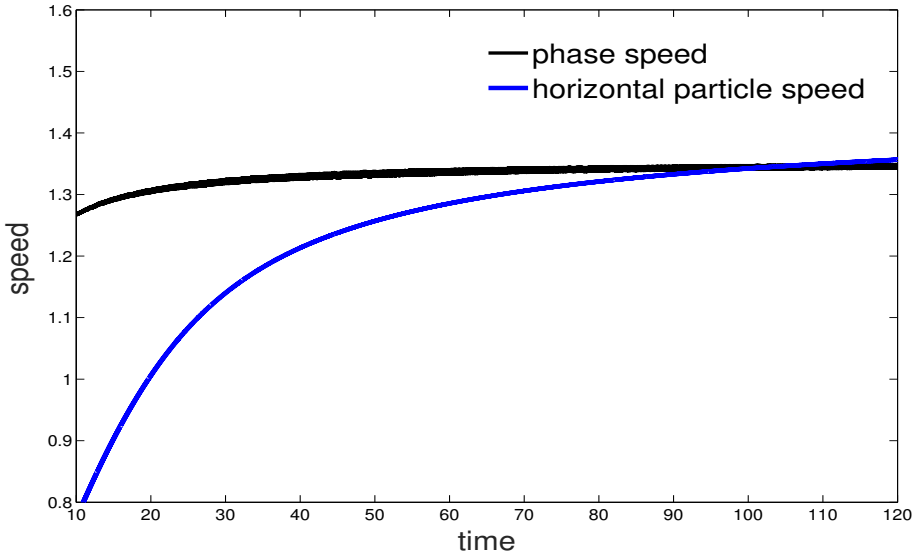

Figure 7.2: Phase speed and horizontal particle speed for $\alpha = 0.355$

As expected, the bore strength for which breaking occurs is bigger than the value found experimentally, but is fairly close to the one obtained using a similar numerical model in [3].

7.2 Computation of critical wave height

In this section we calculate the maximum wave height of the undular bore, using a range of different values of α, starting with the value obtained in the last section, α_{crit}. We expect the maximum height of the bore will be close to the maximum height of the solitary wave, at least if a large number of steps are needed to reach the breaking point. This is because the leading wave of the bore eventually will become a solitary wave, as described in [1].

We find the maximum height of the bore by calculating the phase speed and horizontal particle speed at each time step, as explained in section 6.6, and then find the time at which the two lines cross. The maximum value of the solution may then be extracted at this particular time step to estimate the maximum wave height.

The calculations were done using both the SBP-SAT method and the IFD method. Results are listed in the table below:

	SBP-SAT method		IFD method	
α	$H_{\max}$	Time	$H_{\max}$	Time
0.500	0.722011619835743	5.454	0.724054501182306	5.562
0.490	0.721651568146300	6.129	0.723699016650280	6.248
0.480	0.717175507066406	6.75	0.721179044435669	6.958
0.470	0.714771453439102	7.542	0.716699460888482	7.691
0.460	0.713684376842351	8.517	0.714325398160490	8.633
0.450	0.709583799777383	9.508	0.713009492374458	9.796
0.440	0.705926148989214	10.689	0.709166857513762	11.015
0.430	0.703418165673455	12.177	0.707882844612373	12.664
0.420	0.702812697412847	14.153	0.703965709520160	14.453
0.410	0.697656804566612	16.165	0.701380475310082	16.826
0.400	0.695420951991571	19.096	0.699067340165917	19.966
0.395	0.695106313739639	21.052	0.697907702748518	21.916
0.390	0.694726940061882	23.377	0.696574384496332	24.224
0.385	0.692582691587988	25.803	0.695553952873184	27.141
0.380	0.692335063114321	29.314	0.694411311983090	30.826
0.375	0.690577299203816	33.347	0.693817761385610	35.845
0.370	0.690278926321731	39.451	0.693172891225846	42.900
0.365	0.687981416809282	45.156	0.692539135963483	53.556
0.360	-	-	0.691923925867597	71.473
0.355	-	-	0.690766954393334	105.561

Table 7.1: This table shows the maximum wave height, $H_{\max}$, for corresponding values of α. Calculations were done using both the SBP-SAT method and the implicit FD method.

Both the SBP-SAT method and the implicit FD method yield similar results, and we thus conclude they are working correctly. The figures below shows the solution profiles at the breaking points for $\alpha = 0.5$. The first one is calculated using the SBP-SAT method, and the second one is calculated using the IFD method.

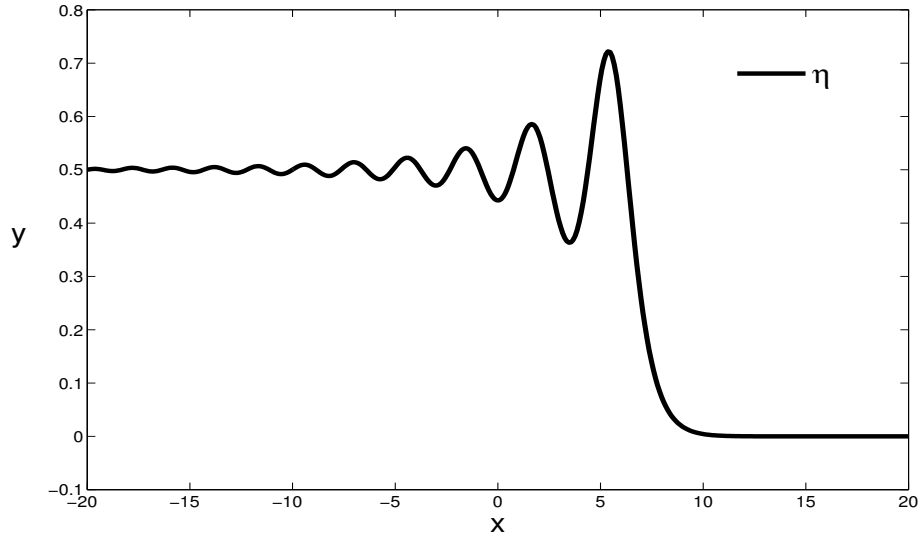

Figure 7.3: Solution profile at breaking point for $\alpha = 0.5$ using the SBP-SAT method.

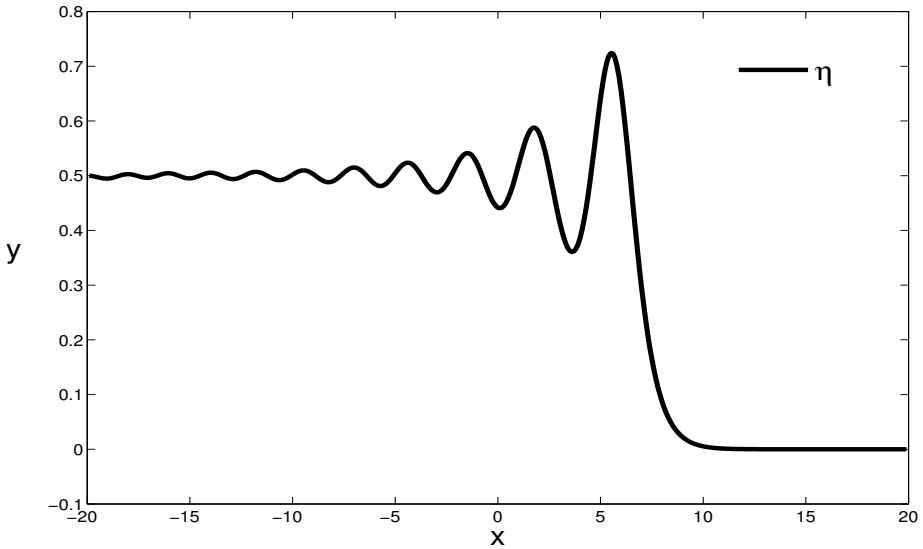

Figure 7.4: Solution profile at breaking point for $\alpha = 0.5$ using the IFD method.

The values obtained for maximum wave height of the bore seems to ap-

proach the maximum height of the solitary wave as the bore strength decreases, and thus increasing the time needed to reach the point of breaking. The figure below shows a plot of the calculated values of $H_{\max}$ using the IFD method, as a function of time. A curve of the form $y_{\text{fit}} = at^b + c$ has also been fitted to the data:

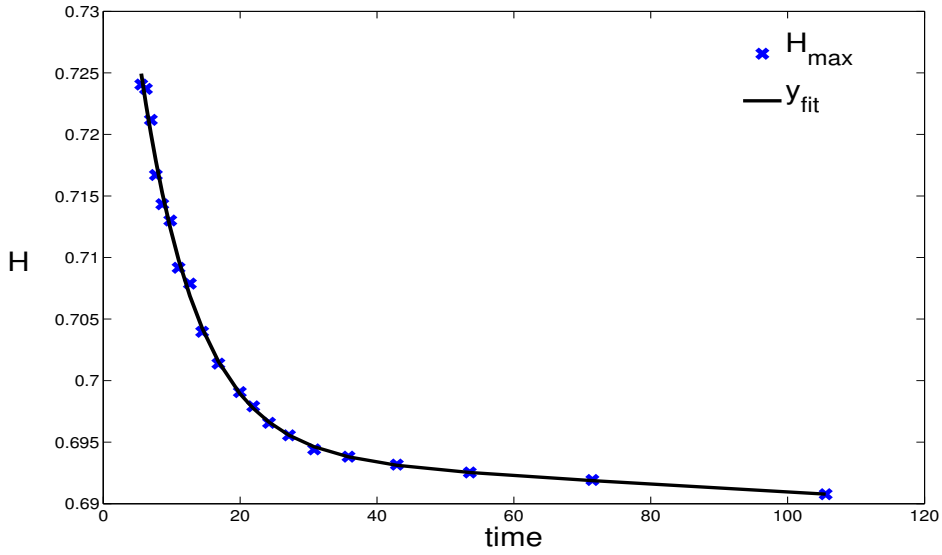

Figure 7.5: Maximum wave height as a function of time

The parameters a, b and c in the fitted curve are given by:

$$a = 0.1764,\ b = -0.8582 \ \text{ and } \ c = 0.6863.$$

Where the sum of squares due to error is: SSE $= 2.54 \cdot 10^{-5}$,
and the R-square and root mean squared error (RMSE) are:
R-square $= 0.9896$ and RMSE $= 0.0012$

The curve fits the data pretty well, and it is evident from the form of the equation that it approaches the value $c = 0.6863$ for large t. This value differs from the maximum height of the solitary wave, $H_{\max \text{ solitary}}$, by: $\Delta = 0.0016$. In addition, we see from the table above that for $\alpha = 0.365$ the SBP-SAT method yields the value $H_{\max} = 0.68798$, which differs from the maximum height of the solitary wave by: $\Delta = 0.00012$, which is even less.

We can therefore confirm that the bore eventually disintegrates into several solitary waves, but as the bore strength, α, increases, the bore will break before this happens and thus can not be described in terms of solitary waves. This also makes it likely that we could obtain a lower value of the critical ratio, α_{crit}, than the one found in the previous section, by using a higher number of time steps, and thus yielding a maximum wave height even closer to that of the solitary wave.

We continue by plotting bore strength as a function of corresponding breaking times, calculated using the IFD method. A curve of the same form as above has also been fitted to the data:

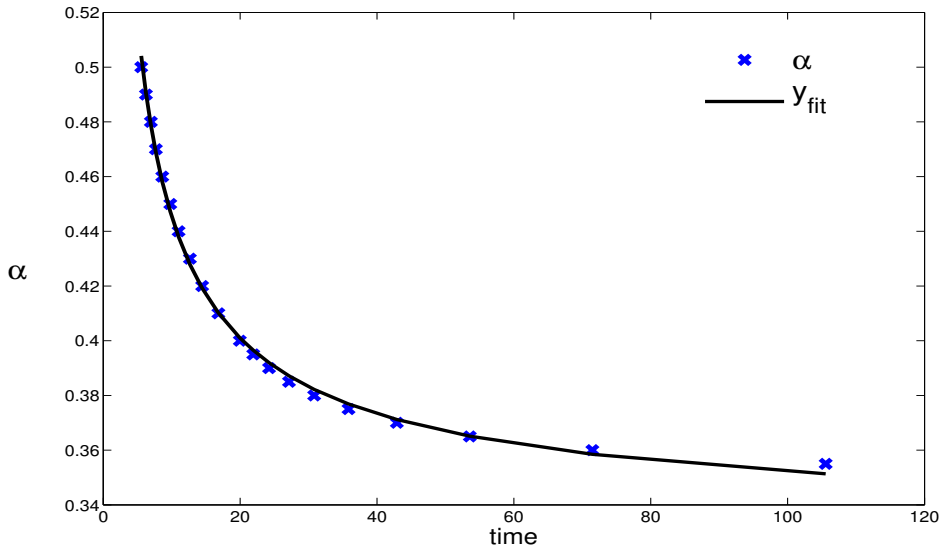

Figure 7.6: Bore strength as a function of corresponding breaking times

The parameters a, b and c in the fitted curve are given by:

$$a = 0.5751, \; b = -0.6908 \;\; \text{and} \;\; c = 0.3283.$$

Where the sum of squares due to error is: SSE $= 7.74 \cdot 10^{-5}$,
and the R-square and root mean squared error (RMSE) are:
R-square $= 0.9979$ and RMSE $= 0.0021$

The fitted curve fits the data pretty well also here, and it will approach the value $c = 0.3283$ for large values of t. This value is somewhat lower than the value of α_{crit} obtained in the previous section. It is possible that the true

value of α_{crit} for this particular model lies somewhere around this value. How many time steps are needed for the bore to exhibit breaking when $\alpha = 0.328$ is, however, another question.

Chapter 8

Conclusions and discussion

In this report we have formulated a breaking criterion for long waves, by using an expression for the horizontal particle speed of the fluid flow. This expression was obtained during the derivation of the Boussinesq system of equations, and is therefore correct to the same order as the KdV equation. The key to this breaking criterion is that the horizontal particle speed only depends on depth and displacement of the surface. This was accomplished in the following steps:

First, the flow potential is expanded around the bottom elevation, and vertical partial derivatives are replaced with horizontal partial derivatives. Differentiating this expansion with respect to the horizontal coordinate yields a similar expansion for the horizontal particle speed.

Then, by restricting the wave motion to only one horizontal direction, terms up to second order in this expansion are replaced with the surface displacement and its spatial derivatives.

This is also how we manage to incorporate the underlying vertical structure of the fluid flow into an equation involving only the surface displacement, namely the KdV equation.

In contrast to the shallow water equations, the KdV equation also includes dispersion. This fact is what allows the solutions to maintain a constant shape, since dispersive effects cancel out the nonlinear effects which would otherwise have caused the waves to change shape. However, due to the nonlinearity of the equation there is still a dependence on propagation speed and wave height. Applying the breaking criteria to these solutions therefore yields a maximum wave height. For the periodic solution the maximum wave height depends on the shape of the wave, and it will approach the maximum height of the solitary wave in the most nonlinear limit. On the other hand, in the linear limit the maximum wave height approaches zero.

This only reflects the approximate nature of the model since no nonlinear effects forces the relative amplitude to become zero.

Moving on to numerical experiments, we then used the breaking criterion to determine the critical ratio, α_{crit} for which the bore first exhibits breaking. This result was somewhat higher than the experimentally determined value, which was obtained using wave tank experiments [7], but lower than the ratio obtained using a similar numerical model in [3]. This is probably not a result of the assumptions made on the physical system, i.e. no transverse motion of the fluid and an irrotational and inviscid flow, since when viscosity is present, the onset of breaking should be delayed compared to the non-viscous case. It therefore seems likely that the limiting procedure used in obtaining the model equations is responsible for some of the discrepancy, although this is only a guess.

It may be possible to obtain a smaller value of α_{crit} using the same model, if a larger number of steps are used in the numerical computation. After interpolating the data points this value was estimated to be around $\alpha = 0.323$. However, since the breaking times seems to grow exponentially for decreasing values of α, it might be hard to actually reach this value through numerical computation. It would be interesting to see if the ratio $\alpha = 0.28$ could be predicted by interpolating the results from a higher order model.

The maximum wave heights of the bore, calculated for a given value of α, all lie slightly above the maximum height of the solitary wave. However, there is a declining trend for longer breaking times. When interpolating these data points, it becomes clear that the bore eventually becomes a train of solitary waves, and the maximum wave height is governed by the maximum height of the solitary wave. This is because of the small difference between the actual value of the maximum height of the solitary wave and the value predicted by the interpolated curve. It seems that for larger values of α, the bore will break before it has enough time to 'become' the solitary wave. If it is possible to predict the maximum height of the bore in these cases remains an open question.

The maximum height obtained by the SBP-SAT method for $\alpha = 0.365$ gives a value even closer to the maximum height of the solitary wave than the value obtained by interpolating the results from the IFD method. It seems therefore that the SBP-SAT method is more accurate than the IFD method. This is likely because of the growing oscillations of the surface at the left boundary, causing the left boundary condition to be inaccurate for

large t, no matter the length of the spatial domain. Since the SBP-SAT method imposes the boundary conditions weakly, this problem is avoided. A better choice for the left boundary condition, which takes into account the growing oscillations, might be necessary for the IFD method to achieve the same degree of accuracy.

Appendix A

Source code for implicit FD method

```
% MatlLab script to solve the problem:
% u_t + u_x + 3/2uu_x + 1/6u_xxx = 0
% u(x,0) = f(x)
% u(-l,t) = alpha
% u(l,t) = 0
% using an implicit FD method

l = 50;                          % length of spatial domain /2
Nx = 1000;                       % number of grid points
dx = 2*l/Nx;                     % uniform spacing between grid points
x = -l+dx:dx:l-dx;               % spatial grid (Nx-1 points)
Nt = 10000;                      % number of time steps
dt = 0.001                       % size of time step
alpha = 0.5;                     % bore strength
k = 1;                           % steepness of initial bore slope

maxvalue = zeros(Nt,1);          % maximum value of solution
maxindex = zeros(Nt,1);          % index of max value
maxpos = zeros(Nt,1);            % position of max value


N = 500;
partspeed = zeros(Nt-2*N,1);     % horizontal particle speed
c = zeros(Nt-2*N,1);             % phase speed
```

```
% time array
t = zeros(Nt,1);
for i = 1:Nt-1
    t(i+1) = i*dt;
end
t2 = t(N+1:Nt-N,1);


D3 = zeros(Nx-1,Nx-1);          % difference matrix for third
                                % derivative.
D1 = zeros(Nx-1,Nx-1);          % difference matrix for first
                                % derivative.
I = eye(Nx-1,Nx-1);             % identity matrix

% build D3:
for i = 3:Nx-3
    D3(i,i-1) = 2;
    D3(i,i-2) = -1;
    D3(i,i+1) = -2;
    D3(i,i+2) = 1;
end
D3(1,1) = 10; D3(1,2) = -12; D3(1,3) = 6; D3(1,4) = -1;
D3(2,1) = 2; D3(2,3) = -2; D3(2,4) = 1;
D3(Nx-1, Nx-1) = 1; D3(Nx-1, Nx-2) = 2; D3(Nx-1, Nx-3) = -1;
D3(Nx-2, Nx-1) = -2; D3(Nx-2, Nx-3) = 2; D3(Nx-2, Nx-4) = -1;
D3 = 1/2/dx^3.*D3;

% build D1:
for i = 2:Nx-2
    D1(i,i+1) = 1;
    D1(i,i-1) = -1;
end
D1(1,2) = 1;
D1(Nx-1,Nx-2) = -1;
D1 = 1/2/dx.*D1;

% RHS
f = alpha/2*(1 - tanh(k*x'));
dxf = -alpha*k/2*sech(k*x').^2;
d3xf = (alpha*k^3*sech(k*x').^2).*(sech(k*x').^2 - 2*tanh(k*x').^2);
```

```
F = -1/6*d3xf - dxf - 3/2*f.*dxf;

% initial condition:
u = f;
temp = zeros(Nx-1,1);

% extract max value and position
[maxvalue(1),maxindex(1)] = max(u);
maxpos(1) = x(maxindex(1));


% matrices used in calculation
E = (I + dt/2*D1 + dt/12*D3);
A = E\(I - dt/2*D1 - dt/12*D3);
B = 3*dt/2*(E\D1);
C = dt*(E\F);


% first time step calculated by forward Euler method:
v = A*temp - B*(1/2*temp.^2 + eta0.*temp) + C;
u = v + f;

% extract max value and position
[maxvalue(2),maxindex(2)] = max(u);
maxpos(2) = x(maxindex(2));

j = 1;
% remaining time steps calculated by A-B and trapezoid method:
for i = 3:Nt
    temp2 = v;
    v = A*v - B*( 3/2*(1/2*v.^2 + f.*v) - 1/2*(1/2*temp.^2 + f.*temp)
    u = v + f;
    temp = temp2;

    % extract max value and position
    [maxvalue(i),maxindex(i)] = max(u);
    maxpos(i) = x(maxindex(i));

   % calculate horizontal particle speed for N<i<Nt-N+1
    if i > N  && i < Nt-N+1
        partspeed(j) = maxvalue(i) - 1/4*maxvalue(i)^2 +...
```

```
        (1/3 - 1/2*(maxvalue(i) + 1)^2)*...
         (u(maxindex(i)-1) - 2*maxvalue(i) + u(maxindex(i)+1) )/dx^2;
        j = j + 1;
    end

end

% smooth out curves
maxpos = smooth(maxpos,400);
u = smooth(u,400);

% phase speed
for i = 1:length(t2)
    c(i) = (1/12*maxpos(i+N-2) - 2/3*maxpos(i+N-1) +...
        2/3*maxpos(i+N+1) - 1/12*maxpos(i+N+2))/dt;
end

% smooth out curve
c = smooth(c,500);

ind = 0;
diff = 1;
% intersection of phase and particle speed
for i = 1:length(t2)
    if abs(c(i) - partspeed(i)) < diff
        ind = i;
        diff = abs(c(i) - partspeed(i));
    end
end


% max value and time at breaking point
maxheight = maxvalue(ind+N);
breaktime = t2(ind);
```

Appendix B

Source code for SBP-SAT method

```
% MatlLab script to solve the problem:
% u_t + u_x + 3/2uu_x + 1/6u_xxx = 0
% u(x,0) = f(x)
% u(-l,t) = alpha
% u(l,t) = 0
% using an SBP–SAT method

l = 50;                          % length of spatial domain /2
Nx = 1000;                       % number of grid points
x = linspace(-l,l,Nx)';          % spatial grid
dx = x(2) - x(1);                % uniform spacing between grid points
Nt = 10000;                      % number of time steps
dt = 0.001                       % size of time step
alpha = 0.5;                     % bore strength
k = 1;                           % steepness of initial bore slope

maxvalue = zeros(Nt,1);          % maximum value of solution
maxindex = zeros(Nt,1);          % index of max value
maxpos = zeros(Nt,1);            % position of max value

N = 500;
partspeed = zeros(Nt-2*N,1);     % horizontal particle speed
c = zeros(Nt-2*N,1);             % phase speed
```

```
% coeffs
a = 3/2;
b = 1/6;

% time array
time = zeros(Nt,1);
for i = 1:Nt-1
    time(i+1) = i*dt;
end
t2 = t(N+1:Nt-N,1);

% initial cond
u = alpha/2*(1 - tanh(x));

% extract max value and position
[maxvalue(1),maxindex(1)] = max(u);
maxpos(1) = x(maxindex(1));

% SBP operators
D = -diag(ones(Nx-1,1),-1) + diag(ones(Nx-1,1),1);
D(1,1) = -2; D(1,2) = 2; D(Nx,Nx) = 2; D(Nx,Nx-1) = -2;
D = D/2/dx;

DD = D*D;
DDD = D*D*D;

PI = diag(ones(Nx,1),0);
PI(1,1) = 2; PI(Nx,Nx) = 2;
PI = 1/dx*PI;

e1 = zeros(Nx,1);
e1(1) = 1;

eN = zeros(Nx,1);
eN(end) = 1;

% boundaries data
g1 = alpha;
gN = 0;
gNx = 0;
```

```
% Runge-Kutta 4 coeffs
RK = dt*[0 1/2 1/2 1];
nstage = 4;
K = zeros(Nx,nstage);

j = 1;
for i = 2:Nt
    uold = u;
    for stage = 1:nstage
        u = uold + RK(stage)*u;

       % direction at boundaries
        al = 1 + a*max(u(1),0);
        ar = 1 + a*min(u(end),0);

        Du = D*u;
        % penalty terms
        SAT1 = -1/2*PI*(al + 2*b*DD')*e1*(u(1) - g1);
        SAT2 = 1/2*PI*(ar + 2*b*DD')*eN*(u(end) - gN);
        SAT3 = -b/2*PI*D'*eN*(Du(end) - gNx);

        u = -D*u - a/2*D*u.^2 - b*DDD*u + SAT1 + SAT2 + SAT3;
        K(:,stage) = u;
    end

    u = uold + dt/6*(K(:,1) + 2*K(:,2) + 2*K(:,3) + K(:,4));

    % extract max value and position
    [maxvalue(i),maxindex(i)] = max(u);
    maxpos(i) = x(maxindex(i));

    % calculate horizontal particle speed for N<i<Nt-N+1
    if i > N  && i < Nt-N+1
        partspeed(j) = maxvalue(i) - 1/4*maxvalue(i)^2 +...
        (1/3 - 1/2*(maxvalue(i) + 1)^2)*...
         (u(maxindex(i)-1) - 2*maxvalue(i) + u(maxindex(i)+1) )/dx^2;
        j = j + 1;
    end


end
```

```
% smooth out curves
maxpos = smooth(maxpos,400);
horvel = smooth(horvel,400);

% phase speed
for i = 1:length(t2)
    c(i) = (1/12*maxpos(i+N-2) - 2/3*maxpos(i+N-1) +...
        2/3*maxpos(i+N+1) - 1/12*maxpos(i+N+2))/dt;
end

% smooth out curve
c = smooth(c,500);

ind = 0;
diff = 1;
% intersection of phase and particle speed
for i = 1:length(t2)
    if abs(c(i) - partspeed(i)) < diff
        ind = i;
        diff = abs(c(i) - partspeed(i));
    end
end


% max value and time at breaking point
maxheight = maxvalue(ind+N);
breaktime = t2(ind);
```

Bibliography

[1] G. B. Witham, *Linear and Nonlinear waves*, John Wiley & Sons (1970)

[2] A. Ali and H. Kalisch, *A dispersive model for undular bores*, Anal. Math. Phys. 2 (2012), p. 347-366

[3] M. Bjørkvåg and H. Kalisch, *Wave breaking in Boussinesq models for undular bores*, Physics Letters A 375 (2011), p. 1570-1578

[4] P. G. Drazin and R. S. Johnson *Solitons: An introduction*, Cambridge University Press (1989)

[5] J. O. Skogestad and Henrik Kalisch *A boundary value problem for the KdV equation: Comparison of finite-difference and Chebyshev methods*, Mathematics and Computers in Simulation Volume 80 (2009), p. 151-163

[6] P. K. Kundu, I. M. Cohen and D. R. Dowling *Fluid Mechanics, fifth edition* Academic Press (2012)

[7] H. Favre *Ondes de Translation* Dunod, Paris (1935)

[8] G. Stokes *On the theory of oscillatory waves* Transactions of the Cambridge Philosophical Society 8 (1847), p. 441?455.

[9] G. B. Airy *Tides and Waves* Encyclopedia Metropolitana (1845)

[10] J. Boussinesq *Théorie des ondes et des remous qui se propagent le long d'un canal rectangulaire hor- izontal, en communiquant au liquide contenu dans ce canal des vitesses sensiblement pareilles de la surface au fond* J. Math. Pures Appl. 17 (1872), p. 55-108

[11] J. Boussinesq *Essai sur la théorie des eaux courantes* l?Acad. des Sci. Inst. Nat. France, (1877)

[12] Lord Rayleigh *On waves* Philos. Mag. Ser. 5 1 (1876), p. 257-279.

[13] D. J. Korteweg and G. deVries *On the change of form of long waves advancing in a rectangular channel, and on a new type of long stationary waves* Philos. Mag. 39 (1895), p. 422-443

[14] N. J. Zabusky and M. D. Kruskal *Interaction of "Solitons" in a collision less plasma and the recurrence of initial states* Phys. Rev. Lett. 15 (1965), p. 240-243

[15] C. S. Gardner, J. M. Greene, M. D. Kruskal and R. M. Miura *Method for solving the Korteweg-deVries equation* Phys. Rev. Lett. 19 (1967), p. 1095-1097

[16] J. S. Russell *Report on waves* Report of the fourteenth meeting of the British Association for the advancements of Science (1844)

[17] H. Borluk and H. Kalisch *Particle dynamics in the KdV approximation* Wave Motion 49 (2012), p. 691-709

[18] M. W. Dingemans *Water wave propagation over uneven bottoms: non-linear wave propagation* World Scientific Pub. (1997) p. 708-715

[19] M. Svärd and J. Nordström *Review of summation-by-parts schemes for initial-boundary-value problems* Journal of Computational Physics Vol. 268 (2014), p.17-38